$$\sigma^{(21)*2}_{\text{on-comp}} = \frac{1}{4}\sum_{ij}^{n}(4L_i^{(2)}\{\langle a_{oi}s_i\rangle^{(2)}-\langle a_{oi}s_i\rangle^{(1)}\}^2\delta_{ij}$$

$$+[\langle a_{oi}a_{oj}s_is_j\rangle^{(2)}-\langle a_{oi}a_{oj}s_is_j\rangle^{(1)}]^2$$

$$\cdot[(L_i^{(4)}-2L_i^{(2)^2})\delta_{ij}+2L_i^{(2)}L_j^{(2)}]) \ ,$$

$$= \sigma^{(21)*2}_{\text{coh}} + \sigma^{(21)*2}_{\text{inc}} \ , \qquad (6.80b)$$

cf. (A.3-35,36). The "small-signal" condition ($\sigma^{*}_{\text{n-comp}} \doteq \sigma^{*}_{\text{on-comp}}$) is given here by the stricter of (6.75), (6.76), or the more special cases, (6.77) vs. (6.78). Performance (P_D^*, P_e^*) is obtained by applying (6.80b) to (6.5a), (6.5e).

--- --- ---

Various suboptimum composite algorithms are suggested as extensions of the previously developed simple and clipper-correlators discussed earlier in this Section (and in Appendix A.4). Thus, parallelling the optimum examples above, we have from A, B of Sec. 4.2 above:

I. Composite Simple Correlators (H_1 vs. H_o):

$$g_{\text{n-comp}} = \log \mu + \hat{B}_{\text{n-comp}} + \frac{1}{2}\sum_{ij}^{n}\{2x_i\langle\theta_i\rangle\delta_{ij}+\langle\theta_i\theta_j\rangle x_i x_j\}, \qquad (6.81a)$$

where

$$\hat{B}_{\text{n-comp}} = -\frac{1}{4}\{\sum_{ij}^{n}(2\{\langle\theta_i\rangle^2+\langle\theta_i^2\rangle\}\delta_{ij}+\langle\theta_i\theta_j\rangle^2). \qquad (6.81b)$$

The H_o-variance of $g_{\text{n-comp}}$ is the sum of the variances (A.4-57), viz.

$$\hat{\sigma}^2_{\text{on-comp}} = \sum_{ij}^{n} \left(\{\langle\theta_i\rangle^2+\left(\frac{\overline{x_i^4}-3}{4}\right)\langle\theta_i\theta_j\rangle^2\}\delta_{ij}+2\langle\theta_i\theta_j\rangle^2\right) \tag{6.81c}$$

II. Composite Clipper-Correlators (H_1 vs. H_o):

$$g_{\text{n-comp}} = \log\mu + \hat{B}_{\text{n-comp}} + \sum_{ij}^{n}(\delta_{ij}\sqrt{2}\langle\theta_i\rangle \operatorname{sgn} x_i+\langle\theta_i\theta_j\rangle \operatorname{sgn} x_i \operatorname{sgn} x_j), \tag{6.82a}$$

where

$$\hat{B}_{\text{n-comp}} = -\frac{1}{4}\sum_{ij}^{n}[4\{(\langle\theta_i\rangle^2-\langle\theta_i^2\rangle)\sqrt{2}\, w_{1E}(0)_i+\langle\theta_i^2\rangle\}\delta_{ij}$$

$$+\langle\theta_i\theta_j\rangle^2[8w_{1E}(0)_i w_{1E}(0)_j-\{\sqrt{2}\, w''_{1E}(0)_i+8w_{1E}(0)_i^2\}\delta_{ij}]] \,. \tag{6.82b}$$

The H_o-variance is the sum of the variances (A.4-68), viz:

$$\hat{\sigma}^2_{\text{on-comp}} = \sum_{ij}^{n}(\{2\langle\theta_i\rangle^2-\langle\theta_i^2\rangle^2\}\delta_{ij}+2\langle\theta_i\theta_j\rangle^2) \,. \tag{6.82c}$$

The "small-signal" conditions here are the stricter of (A.4-59) for the simple correlators, and the stricter of (A.4-70) in the case of the clipper-correlators.

For performance in the above (and generally), we need both $\hat{\sigma}^2_{\text{on-comp}}$ and the quantity $\sigma_{\text{o-comp}}$, defined by

$$\frac{\langle g_{\text{comp}}\rangle_1-\langle g_{\text{comp}}\rangle_o}{\sqrt{2}\,\hat{\sigma}_{\text{on-comp}}} = \frac{[\text{numerator of (A.4-12a,b)+numerator of A.4-31a,b)}]}{\sqrt{2}\,[\{\text{Eq. (A.4-9)+Eq.(A.4-29)}\}=\hat{\sigma}^2_{\text{on-comp}}]^{1/2}}$$

$$\equiv \frac{\sigma_{\text{o-comp(F)}}}{\sqrt{2}} \,, \tag{6.83a}$$

and

$$\frac{\langle g_{comp}\rangle_1}{\sqrt{2}\,\hat{\sigma}_{on\text{-}comp}} = \frac{-\langle g_{comp}\rangle_0}{\sqrt{2}\,\hat{\sigma}_{on\text{-}comp}} = \frac{\sigma_{o\text{-}comp(F)}}{2\sqrt{2}} \,. \tag{6.83b}$$

Then, in particular, for these composite correlation detectors we use the results of Appendices A.4-2,3 to obtain the specific values of $L^{(2)}_{F:E}$, $\hat{L}^{(2)}_{F:E}$, etc. which appear in both σ_0,(6.83a,b),and in $\hat{\sigma}^2_{on\text{-}comp}$ (cf. (6.81c), (6.82c)). Performance is then calculated using these values in (6.2)-(6.5), as appropriate. [We recall [D, Sec. A.4-1] that these suboptimum algorithms become optimum against the appropriate noise, e.g. gauss for the simple correlators, "Laplace" noise for the clipper-correlators.

All these (optimum) algorithms are, of course, LOBD's: each gives the minimum error probabilities for all values of input signal ($\theta = \sqrt{\overline{a^2}}$) in some finite range $0 < \theta < \epsilon(<<1)$. But each LOBD has a different range, e.g. $\epsilon_{coh} \neq \epsilon_{inc} \neq \epsilon_{comp}$; in fact, $\epsilon_{comp} \geq \epsilon_{coh} \geq \epsilon_{inc}$, since $LOBD_{comp}(\bar{\theta}\geq 0)$ is never worse than $LOBD_{coh}$, which in turn is never inferior to $LOBD_{inc}$, for the same common channel conditions, provided the input signal level ($\sim a_o^2$) is not too great (i.e. the "small-signal" conditions). For very small signals we may expect that $LOBD_{comb} \to (LOBD)_{coh}$, $(\bar{\theta}>0)$, since the incoherent component $(0<\theta^2<<\bar{\theta})$ is now negligible vis-à-vis the coherent contribution. On the other hand, if $\bar{\theta}=0$, $\therefore (LOBD)_{coh}=0$, and $LOBD_{comp}=(LOBD)_{inc}$, with the range ϵ_{inc}.

Finally, the composite LOBD is generally recommended, provided the complexity of the processing occasioned by the additional algorithmic component ($LOBD_{inc}$, or $LOBD_{coh}$) can be tolerated practically. Otherwise, in the coherent cases we omit the $(LOBD)_{inc}$-component; hence the considerable attention to the coherent algorithm ($\bar{\theta}>0$) now and previously. [It is, of course, analytically much simpler than $(LOBD)_{inc}$, which can be an additional reason to focus on $(LOBD)_{coh}$ when $\bar{\theta}>0$.] As noted in Sec. A.3-(I,II), a rare special situation arises in the gaussian case for the completely known signals: the

composite LOBD is replaced by the exact, $(\text{LOBD})_{coh}$ form. When the noise is non-gaussian, we proceed as above.

III. Composite Threshold Detectors: Minimum Detectable Signals:

We conclude Sec. 6.5 with a derivation of the minimum detectable signal for these optimum composite threshold cases. Combining (6.9) and (6.22b), for example, remembering from (6.79c) that $\sigma^{*2}_{\text{on-comp}} = \sigma^{*2}_{\text{on-coh}} + \sigma^{*2}_{\text{on-inc}}$, we can define at once (in these "on-off" cases with stationary noise) $\left\langle a_o^2 \right\rangle^*_{\text{min-comp}}$ by

$$\sigma^{*2}_{\text{on-comp}} \equiv 2 \left\langle a_o^2 \right\rangle^*_{\text{min-comp}} \hat{a}_{coh} \Pi^*_{coh} + 2 \left\langle a_o^2 \right\rangle^*_{\text{min-comp}} \hat{a}^2_{inc} \Pi^*_{inc} \tag{6.84}$$

From (6.2) or (6.4) we get directly

$$\frac{\sigma^*_{\text{on-comp}}}{\sqrt{2}} = 2\Theta^{-1}(1-2P^*_e) \text{ , or } \{\Theta^{-1}(2p^*_D-1)+\Theta^{-1}(1-2\alpha^*_F)\} \equiv C_{\text{I.O.}} \text{ or } C_{\text{N.P.}}, \tag{6.85}$$

$$\equiv \sqrt{B^*_{\text{I.O.}}} \qquad \equiv \sqrt{B^*_{\text{N.P.}}}$$

respectively for the Ideal Observer or the Neyman-Pearson Observer, cf. (6.11b). Applying (6.85) to (6.84), we obtain the desired expression for the minimum detectable signal associated with this "on-off" composite detector, viz.

$$\left\langle a_o^2 \right\rangle^*_{\text{min-comp}} = \frac{1}{2} \frac{\hat{a}_{coh} \Pi^*_{coh}}{\hat{a}^2_{inc} \Pi^*_{inc}} \left\{ \sqrt{1+4B^* \frac{\hat{a}^2_{inc} \Pi^*_{inc}}{\hat{a}_{coh} \Pi^*_{coh}}} - 1 \right\}, \tag{6.86}$$

$$B^* = C^2_{\text{I.O.}} \text{ or } C^2_{\text{N.P.}} ,$$

or, using (6.10), (6.24), with (6.49)', we get explicitly in these stationary cases

$$\left\langle a_o^2\right\rangle^*_{\text{min-comp}} = \frac{4L^{(2)}(1-\eta)}{L^{(4)}+2L^{(2)^2}(Q_n-1)} \left\{ \sqrt{1+\frac{B^*\{L^{(4)}+2L^{(2)^2}(Q_n-1)\}}{2nL^{(2)^2}}} - 1 \right\} . \quad (6.86a)$$

For example, in the case of signals with incoherent structure, $Q_n=1$, and $\therefore\ \Pi^*_{coh}\to 0$:

$$\therefore\ \left\langle a_o^2\right\rangle^*_{\text{min-comp}} = \sqrt{\frac{B^*}{\Pi^*_{inc}}} = \left\langle a_o^2\right\rangle^*_{\text{min-inc}} \quad (6.87a)$$

$$= \sqrt{B}\,\frac{4}{\sqrt{2L^{(4)}_n}} \quad . \quad (6.87b)$$

Similarly, for signals with coherent structures, e.g., sinusoidal pulse trains where $Q_n \doteq n/2$, or $\doteq n(1-\eta)^2/2$, cf. (A.2-42e), for slow or rapid fading respectively and large sample ($n>>1$), we get from (6.86a)

Coh. struct.:

$$\therefore\ \left\langle a_o^2\right\rangle^*_{\substack{\text{min-comp}\\ \text{slow}}} \cong \frac{4(1-\eta)}{nL^{(2)}} \left\{ \sqrt{1+B^*/2(1-\eta)^2} - 1 \right\} \quad (6.88a)$$

$$\cong \frac{4}{nL^{(2)}} \left\{ \sqrt{\frac{B^*}{2}} - (1-\eta) \right\} \quad ;\ B^*>>2(1-\eta)^2 ,$$

$$\left\langle a_o^2\right\rangle^*_{\substack{\text{min-comp}\\ \text{rapid}}} \cong \frac{4}{nL^{(2)}(1-\eta)} \{\sqrt{1+B^*/2} - 1\} \cong \frac{4}{nL^{(2)}(1-\eta)} \left(\sqrt{\frac{B^*}{2}} - 1\right), \quad (6.88b)$$

$$B^*>>2 .$$

Note the expected relations $\left\langle a_o^2\right\rangle^*_{\text{min-comp}\,|\,\text{incoh.struct}} \sim 1/\sqrt{n}$, while $\left\langle a_o^2\right\rangle^*_{\text{min-comp coh.struct.}} \sim 1/n$ cf. remarks in Sec. 6.2, V, (iii), (iv).

The above relation (6.86) also applies for minimum detectable signals in the binary signal cases when $a_o^{(1)} = a_o^{(2)} = a_o$, and no or slow fading with suitable adjustments for $\Pi^*_{coh} \to \Pi^{(21)*}_{coh}$, etc., cf. Table 6.1b. We have explicitly

Binary "Symmetrical" Signals:

$$\langle a_o^2 \rangle^{(21)*}_{min\text{-}comp} = \frac{2(1-\eta)}{L^{(2)}[\hat{Q}_n^{(21)}-1]} \left\{ \sqrt{1+\frac{4B^*(\hat{Q}_n^{(21)}-1)}{\eta}} - 1 \right\} \tag{6.89}$$

with reductions similar to (6.87b), (6.88), depending on $\hat{Q}_n^{(21)}$, cf. (6.33a), (A.6-5c).

Finally, we observe in these optimum threshold cases that the only condition on the AO character of these LOBD's is the equal-variance condition: $x_{max} << x_o^*$; $y_{max}^* << y_o^*$, cf. Fig. 6.1 and Sec. 6.4. Usually, $y_{max} << y_o^*$ is the stricter constraint; i.e., $y_o^* < x_o^*$. (This observation is also consistent with our discussion of III, Sec. 6.4.)

A. Remarks on Suboptimum Composite Threshold Detectors:

This situation is more complex than in the optimum cases above. To obtain the minimum detectable signal when the composite threshold detection is not optimum, we start with (6.83a), to write

$$\sigma^2_{o\text{-}comp}/2 = \frac{[(A.4\text{-}12a)numerator+(A.4\text{-}31a)numerator]^2}{2[(A.4\text{-}9)+(A.4\text{-}29)]^2 \equiv (2\hat{\sigma}^2_{o\text{-}comp})} \tag{6.90}$$

$$= \frac{\langle g_{comp} \rangle_1 - \langle g_{comp} \rangle_2}{2\hat{\sigma}^2_{o\text{-}comp}} ,$$

which defines $\sigma^2_{o\text{-}comp}$. Specifically, for the stationary cases we have

$$\sigma_{o\text{-comp}}/\sqrt{2} = \frac{L^{(2)}_{F:E}\sum_i\langle\Theta_i\rangle^2 + \frac{1}{4}\sum_{ij}\langle\Theta_i\Theta_j\rangle^2\left[\left(\hat{L}^{(4)} - 2L^{(2)^2}\right)\delta_{ij} + 2L^{(2)^2}\right]_{F:E}}{\sqrt{2}\left\{\hat{L}^{(2)}_{F:E}\sum_i\langle\Theta_i\rangle^2 + \frac{1}{4}\sum_{ij}\langle\Theta_i\Theta_j\rangle^2\left[\left(L^{(4)} - 2\hat{L}^{(2)^2}\right)\delta_{ij} + 2\hat{L}^{(2)^2}\right]_{F:E}\right\}}, \quad (6.91)$$

where $\sigma_{o\text{-comp}}/\sqrt{2}$ is used in (6.2) or (6.5) to obtain performance for these suboptimum composite cases. [See Sec. C of Appendix A.4-1 for the $L_{F:E}$'s.]

Now, since $\langle\Theta_i\rangle = \bar{a}_o\sqrt{2}$, $\langle\Theta_i\Theta_j\rangle = \overline{a_o^2}m_{ij}\rho_{ij}$, here, Eq. (6.91) can be written

$$\frac{\sigma_{o\text{-comp}}}{\sqrt{2}} = \frac{\overline{a_o^2}A_1 + \overline{a_o^2}^2 A_2}{\sqrt{2}\left(\overline{a_o^2}B_1 + \overline{a_o^2}^2 B_2\right)^{1/2}} = \sqrt{B^*} \quad , \quad \text{cf. (6.11,6.11a,b).} \qquad (6.92)$$

To obtain the associated minimum detectable signal $\left\langle a_o^2\right\rangle_{\text{min-comp}}$ $(=\overline{a_o^2})$ we must solve (6.92) for $z = \overline{a_o^2}$, e. g.

$$\boxed{z^3A_2^2 + 2A_1A_2z^2 + (A_1^2 - B_1B_2)z - B^*B_1 = 0} \quad , \qquad (6.93)$$

which we leave to a subsequent study. The associated processing gain here is now defined by

$$\Pi_{\text{comp}} \equiv B^*\Big/\left\langle a_o^2\right\rangle^2_{\text{min-comp}} \quad , \qquad (6.94)$$

since

$$\sigma^2_{o\text{-comp}} \equiv 2\left\langle a_o^2\right\rangle^2_{\text{min-comp}}\Pi_{\text{comp}} \quad .$$

7. QUANTITATIVE EXAMPLES: DETECTOR PERFORMANCE

In this Section we examine some specific examples, to illustrate the general results of the preceeding sections, in particular, Section 6. Our general aim is to provide a reasonable catalogue of common signal types, channel conditions, reception modes, and noise models from which to select representative applications.

We begin with a (partial) summary of the results of Sec. 5.3 preceding:

7.1 Statistical-Physical Components of the Receiver Algorithms:

Both to implement the various optimum and suboptimum detection algorithms and to evaluate and compare their performance, we need the structural elements of signal and noise which determine how the received data are to be processed and how these various receivers perform. Accordingly, we note the following typical relations:

I. Common Signal Types

(i). "On-off": $s_i^{(2)}=\sqrt{2}\cos(\omega_o t_i-\phi_o)=\sqrt{2}\cos\omega_o t_i$ (7.1)

$s_i^{(1)}=0$

(ii). Orthogonal: $s_i^{(2)} = \sqrt{2}\cos\omega_o t_i$; (7.2)

$s_i^{(1)}=\sqrt{2}\sin\omega_o t_i$ $(=\sqrt{2}\cos(\omega_o t_i-\pi/2)$

(iii). Antipodal: $s_i^{(2)}= -s_i^{(1)}(=-\sqrt{2}\cos\omega_o t_i)$. (7.3)

} for coherent reception

For incoherent reception we cannot use these RF phase distinctions, and most simply we change the frequency:

$$s_i^{(1)} = \sqrt{2}\cos\omega_{o1}t_i \; ; \; s_i^{(2)} = \sqrt{2}\cos\omega_{o2}t_i \quad . \tag{7.3a}$$

II. Common Channel Conditions:

(1). Fading :

(i). no fading:

$$m_{ij}\,\overline{a_o^2} = a_o^2 = G_o^2/\bar{I}_N\lambda^{2\gamma}\ ;\ (m_{ij}=1) \tag{7.4a}$$

(ii). slow fading (one-sided):

$$m_{ij}\,\overline{a_o^2} = \overline{a_o^2} = \overline{a^2}\langle G_o^2\rangle/\bar{I}_N\lambda^{2\gamma};\ (m_{ij}=1)\ ; \tag{7.4b}$$

(iii). rapid fading (one-sided):

$$m_{ij}\overline{a_o^2} = \overline{a_o^2}[\delta_{ij}+(\bar{a}_o^2/\overline{a_o^2})(1-\delta_{ij})]\ , \tag{7.4c}$$

$$= [\overline{a^2}\ \delta_{ij}+\bar{a}^2(1-\delta_{ij})]\langle G_o^2\rangle/\bar{I}_N\lambda^{2\gamma}\ ; \tag{7.4d}$$

(iv). rapid fading (two-sided):

$$m_{ij}\overline{a_o^2} = \overline{a_o^2}\delta_{ij} = \overline{a^2}\langle G_o^2\rangle/\bar{I}_N\lambda^{2\gamma}\ \ ;\ \bar{a}_o = 0, \tag{7.4e}$$

cf. (5.8), (5.8a), and where the fading effects are represented by the statistics of $\underline{a}$ [cf. (3.3) for rayleigh fading]; $\bar{I}_N$ is the mean intensity of the accompanying noise (cf. Sec. 3.2). Fading is usually the result of unresolvable multipath effects. [For random signal source locations we replace $\lambda^{-2\gamma}$ by $\langle\lambda^{-2\gamma}\rangle$ in (7.4), cf. (3.4),(3.5).]

(2). Doppler:

$$s_i = \sqrt{2}\cos[(\omega_o+\omega_d)t_i-\phi_o]\ ; \tag{7.5a}$$

$$\therefore\ \overline{s_i} = \sqrt{2}\,e^{-(\Delta\omega_d t_i)^2/2}\cos(\omega_o t_i-\phi_o)\ ;\ \Delta\omega_d=\omega_o\Delta v/c_o\ , \tag{7.5b}$$

$$\rho_{ij} = \overline{s_i s_j} = e^{-[\Delta\omega_d(t_i-t_j)]^2/2}\cos\omega_o(t_i-t_j),\ \text{cf.(5.13)}, \tag{7.5c}$$

these last two relations on the assumption that the doppler shift (ω_d) is governed by a gaussian process, cf. Sec. 5.3, Eqs. (5.12) et seq. Without doppler, (7.5) reduce directly to simpler forms, where $\omega_d=0$; $\Delta\omega_d=0$.

(3). Propagation Law (γ):

This will depend on the mean propagation conditions, including the relevant geometry. For instance, simple spherical spreading is represented by $\gamma=1$, while cylindrical spreading (associated with "wave-guide" modes of propagation) is usually $\gamma= 1/2$. Resolvable multipath effects give $\gamma>1$: $\gamma=2$ is typical of rough terrain, cities, etc.; for very rough terrain with multiple reflections, $\gamma>2$. [See Sections 3.1-3.3 above.]

III. Common Modes of Reception:

We distinguish: (i), coherent; (ii), incoherent; and (iii), "mixed" or "composite". "Coherent" reception here implies complete knowledge of the signal epoch (ϵ) [or phase ($\omega_o\epsilon_o$) in the narrow-band cases] at the receiver, and is usually achieved after the desired signal has been originally detected, and "lock-on" in phase has been accomplished. Initial signal detection, of course, is done incoherently, where the ignorance of signal epoch or phase is such that $\langle s \rangle_\epsilon = 0$, with $\rho_{ij} \neq 0$ generally. The composite mode of reception combines both coherent and incoherent processing whenever $\bar{s} \neq 0$, i.e., whenever there is enough phase coherence to provide a non-vanishing mean signal. This occurs both at the intermediate stages of detection and after the coherent mode has been established by successful "lock-on". If one is willing to support the added complexity of the incoherent processing after coherency has been achieved, then "composite" processing (of the kind discussed in Sec. 6.5) provides improved performance over purely coherent (or incoherent) detection alone, cf. the examples (Sec. 7.5) below. Various schema of signal processing are shown in Sec. 5 earlier.

IV. Common Noise Models:

The principle noise or interference models of practical importance are the Class A and B noise models, described in some detail in Sec. 3.3 preceding. The former is "coherent", i.e., produces negligible transients

in the receiver, while the latter is "impulsive", generating essentially nothing but overlapping transient responses. Included with both these primary nongaussian noise mechanisms is an additive gaussian component, partially internal and partially external. The gauss noise model is itself a limiting case of either the Class A or B sources, when the number of independently emitting sources becomes large, or when no individual source stands out above the general gaussian background. It is the Class A and B models which most effectively represent real-world EMI environments and which we consider here specifically below in the application of our general threshold theory to typical EMI examples, both for detector design, i.e. specification of the optimum threshold algorithms, and for the evaluation of performance, including that of suboptimum systems like the simple- and clipper-correlators of conventional practice.

In a compact way, we can summarize typical received narrow-band signal waveforms in common use by the normalized expression

$$s_i^{(\ )} = \sqrt{2}\, a_d(t_i)\cos[(\omega_{o(\ )}+\omega_d)t_i-\phi_o],\ (\ ) \equiv (1),(2), \tag{7.6}$$

where

$$\begin{cases} \phi_o=0 \text{ ("on-off") and } s_i^{(1)}=0;\ =\pi/2 \text{ ("orthogonal")};\ =\pi \text{("antipodal")}, \\ \qquad \text{cf. Eqs. (7.1)-(7.3), in the coherent cases when } \bar{s}_i\neq 0, \text{ only.} \qquad (7.6a) \\ a_d(t_i) = 1 \text{ [no doppler spread), } \omega_d=0 \text{ or } \omega_d\neq 0.] \\ \qquad = e^{-(t_i\Delta\omega_d)^2/2} \quad \text{(gauss doppler spread, } \bar{\omega}_d=0). \qquad (7.6b) \end{cases}$$

The effects of fading (cf. B above) are embodied in the first and second order amplitude statistics $\bar{a}_o$, $\overline{a_o^2}$, viz., $\overline{a_o^2 m_{ij}^{(\ )}}$, where $m_{ij}^{(\ )} \equiv \langle a_{oi}^{(\ )} a_{oj}^{(\ )} \rangle / \overline{a_o^2}^{(\ )}$. In all the binary signal cases henceforth we shall employ the same signal levels, so that $a_o^{(2)} = a_o^{(1)} = a_o$, [but $s^{(2)} \neq s^{(1)}$, of course]. Thus, from (7.4) we have

$$\left.\begin{aligned} m_{ij} &= 1\text{: (no fading, slow, one-sided fading)} ; \\ m_{ij} &= \delta_{ij}+(\bar{a}_o^2/\overline{a_o^2})(1-\delta_{ij})\text{: (rapid fading)}; \\ m_{ij} &= \delta_{ij}\text{: (rapid, two-sided fading)}. \end{aligned}\right\} \tag{7.7}$$

Also, for the signal correlation function $\rho_{ij}^{(\ )}$ we have various possibilities:

$$\left.\begin{aligned} \rho_{ij}^{(\ )} &= \bar{s}_i^{(\ )}\bar{s}_j^{(\ )}\text{: (coherent reception, no doppler, } a_d=1, \omega_d=0); \\ &= \cos \omega_{o(\ )}(t_i-t_j)\text{: (incoherent reception, no doppler)}; \\ &= \exp\{-[\Delta\omega_d\ (t_i-t_j)]^2/2\} \cos \omega_o(t_i-t_j): \\ &\quad \text{(doppler spread, coherent or incoherent reception; } \bar{\omega}_d=0) \end{aligned}\right\} \tag{7.8}$$

Various combinations of (7.6)-(7.8) provide a wide range of typical received signal structures, to be used in obtaining both the algorithmic structure (Secs. 4, 5) and performance results (Sec. 6) when specific numerical results are desired.

7.2 Optimum Structures:

These are described in canonical form in Sections 4, 5. Using A.- D. above in these structural forms, along with $\ell(x_i|A)$, $\{x_i\}$, gives the desired algorithm when combined with a suitable threshold. Thus, ℓ_i exhibits the basic input-output relation for the sampled data $\{x_i\}$.

For Class A interference we have directly

$$\ell(x_i|A) \equiv \frac{d}{dx} \log w_1(x)_{A+G}\Big|_{x=x_i}, \tag{7.9}$$

where $w_1(x)_{A+G}$ is given by (3.13) or (3.14).

Class B interference requires some adjustments, to account for the fact that the parameter Ω_B, cf. (3.15), normalizes the data to the measured value of the (total) intensity, rather than to the calculated value $(\Omega_{2B}+\sigma_G^2)$, which is not obtainable in finite magnitude from the approximation $w_1(x)_{B+G}$, (3.15). Thus writing

$$\hat{x} \equiv x/\sqrt{\Omega_B} = X/\sqrt{(\Omega_{2B}+\sigma_G^2)} \cdot \sqrt{\Omega_B} \ , \tag{7.10}$$

we have $\hat{x}$ now the normalized data (X) with respect to the measured intensity. The pdf (3.15) becomes

$$w_1(\hat{x})_{B+G} \cong \frac{e^{-\hat{x}^2}}{\pi} \sum_{n=0}^{\infty} \frac{(-1)^n}{n!} \hat{A}_\alpha^n \Gamma(\tfrac{n\alpha+1}{2}) {}_1F_1(-\tfrac{n\alpha}{2}; 1/2; \hat{x}^2) \tag{7.11a}$$

$$\simeq \frac{1}{\pi} \sum_{n=0}^{\infty} \frac{(-1)^n}{n!} \hat{A}_\alpha^n \Gamma(\tfrac{n\alpha+1}{2}) {}_1F_1(\tfrac{1+n\alpha}{2}; 1/2; -\hat{x}^2) \ . \tag{7.11b}$$

The (macro-) parameters here are $\hat{A}_\alpha \sim A_B^{1-\alpha/2}$, cf. (3.16b), and $\alpha(=\frac{2-\mu}{\gamma})$, cf. (3.14c), where (μ,γ) are parameters associated with the EMI scenario, cf. (3.6). The basic input-output relation ℓ_i is now

$$\ell(x_i|B) \equiv \frac{d}{dx} \log w_1(x)_{B+G}\Big|_{x=x_i} \tag{7.12}$$

for these Class B cases.

Figures 7.1 and 7.2 show $\ell(x_i|A)$, $\ell(x_i|B)$ for typical parameter values: $\mathcal{P}_{2A}(A_A, \Gamma_A')$, $\mathcal{P}_{2B}(\hat{A}_\alpha, \alpha)$; see Sec. 7.5 for some further comments.

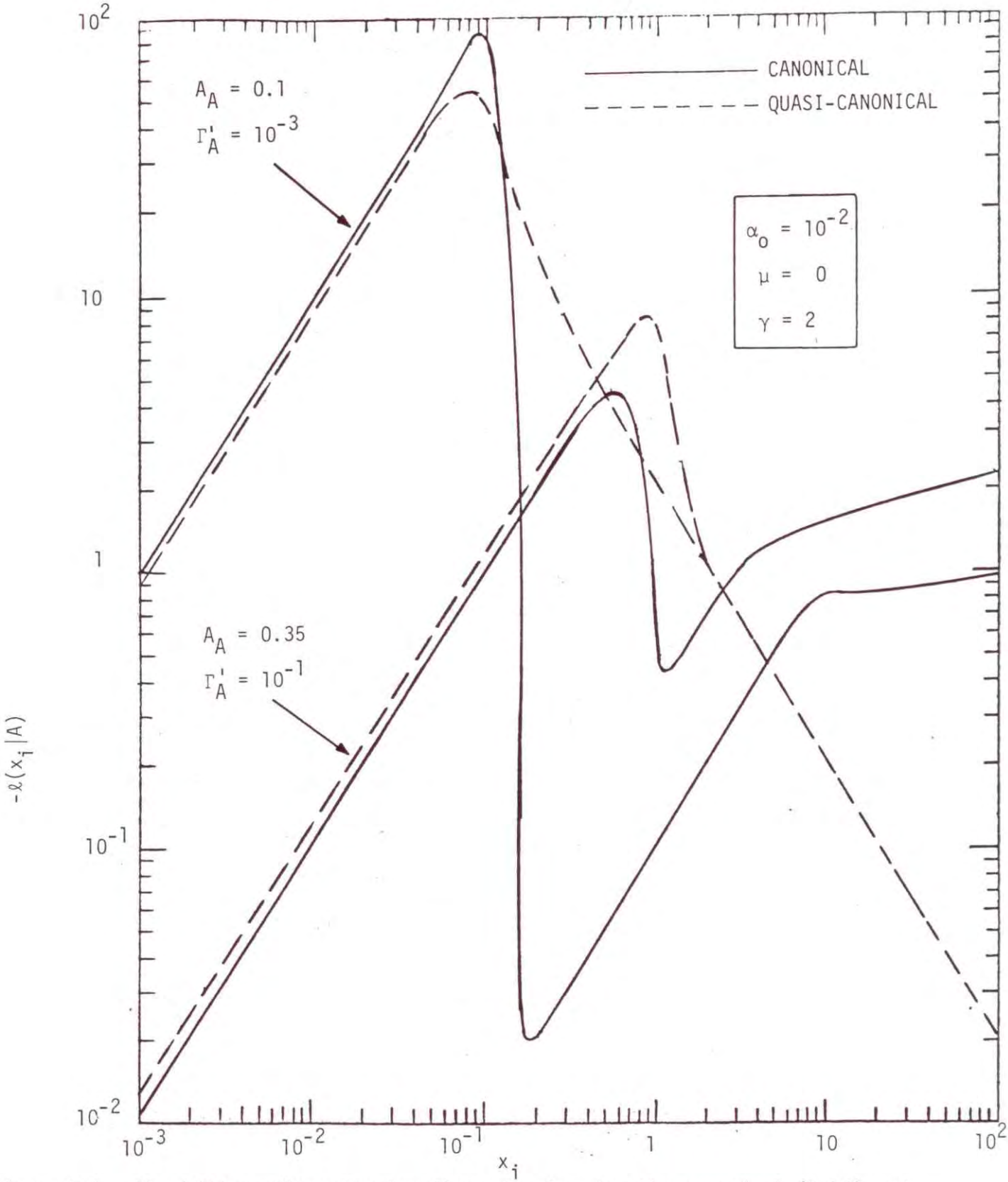

Figure 7.1. The LOBD nonlinearity for Class A noise for the canonical (3.13) and quasi-canonical (3.14) models.

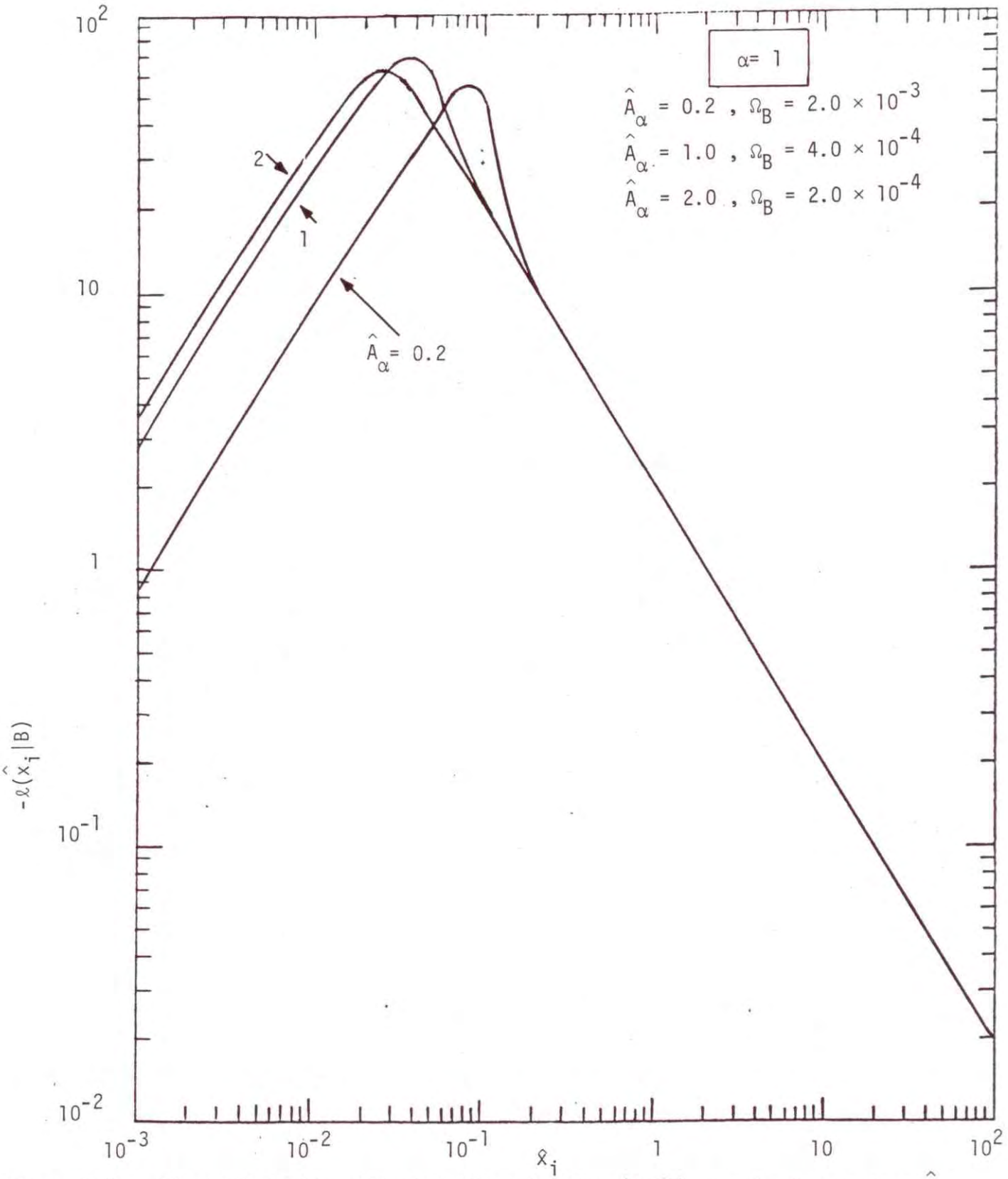

Figure 7.2a. The LOBD nonlinearity for Class B noise (3.15), $\alpha = 1$, for various $\hat{A}_\alpha$.

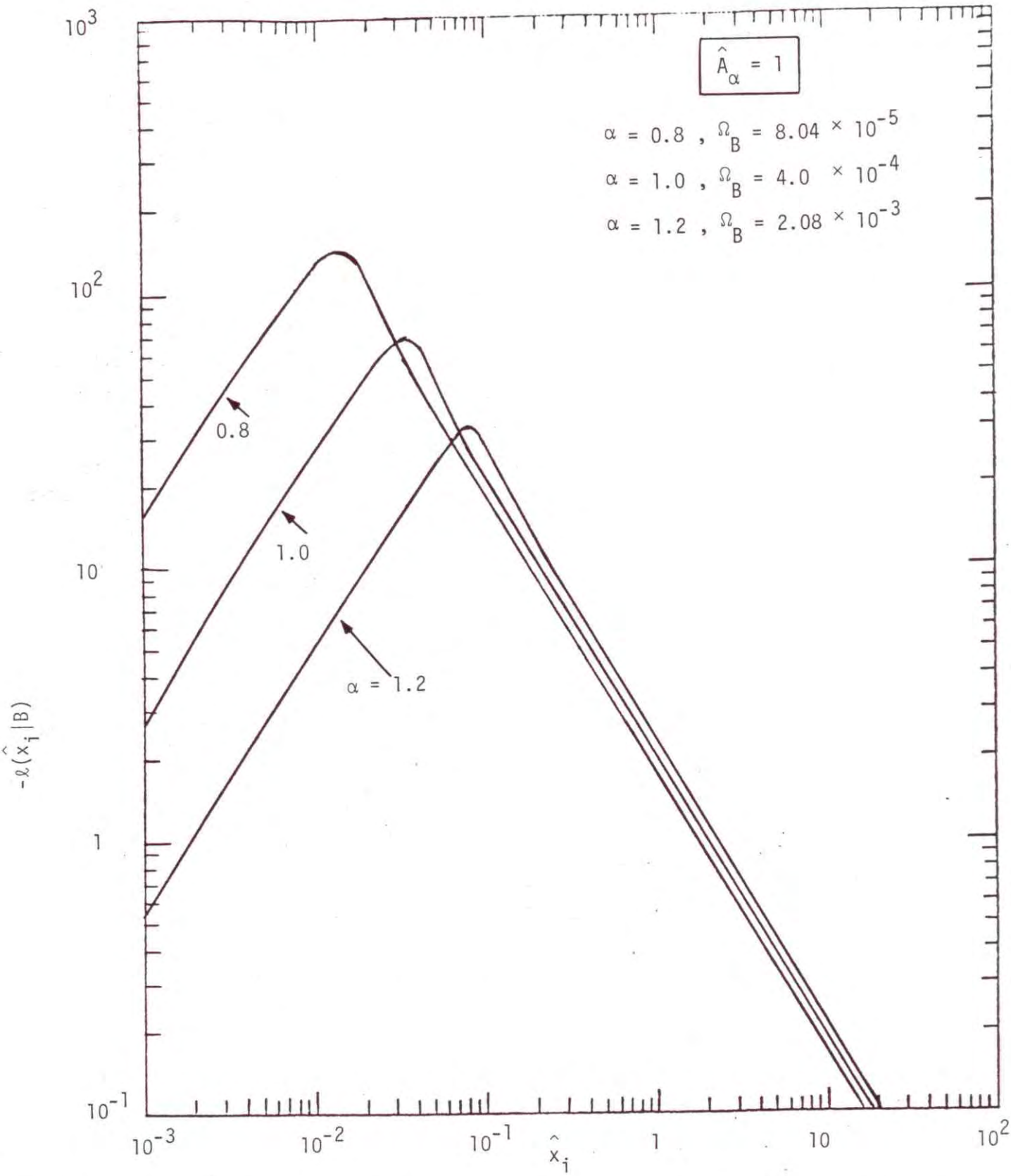

Figure 7.2b. The LOBD nonlinearity for Class B noise (3.15), $\hat{A}_\alpha = 1.0$, for various α.

7.3 Optimum Threshold Detectors: Performance Elements:

Rather than attempting an exhaustive (and expensive) enumeration of all combinations of typical signal, noise, and observational procedures (reviewed in Sec. 7.1 above), we shall adopt the following general approach to obtaining specific numerical results: We shall calculate various canonical relations and "basic ingredients" (e.g., $L^{(2)}$, $L^{(4)}$, etc.), including processing gains (per unit sample) and the appropriate (upper) "bounds" on the magnitude of the input signal associated with both coherent and incoherent detection, as well as such special relations as appear necessary to enhance the usefulness of these results. This procedure we repeat in Section 7.4 for the two classes of suboptimum receiver discussed here, viz., the simple correlator and the clipper-correlator. Thus Section 7.5 is devoted to selected numerical illustrations of performance, including detector comparisons, for typical EMI and signal situations, showing how one may use the canonical results and "basic ingredients" computed initially.

I. Various Useful Canonical Performance Relations:

Independent of the particular noise and signal structures are the probability measures of optimum threshold performance (in large sample régimes), given in Sec. 6.1. Accordingly, we have [cf. footnote, p. 55].

$$P_D^{(*)} \underset{\sim}{=} \frac{p}{2}\left\{1+\Theta\left[\frac{\sigma_{on}^{(*)}}{\sqrt{2}} - \Theta^{-1}(1-2\alpha_F^{(*)})\right]\right\} \quad ;$$

$$P_e^{(*)} \underset{\sim}{=} \frac{1}{2}\left\{1-\Theta\left[\frac{\sigma_{on}^{(*)}}{2\sqrt{2}}\right]\right\} \quad ; \ (\mathcal{A}=\mu=1) \qquad (7.13)$$

from (6.2), (6.5), (6.5e), where the quantity $\sigma_{on}^{(*)}$ $[=(\mathrm{var}_0 g_n^{(*)})^{1/2}]$ is determined in detail according to Sections 6.2-6.5, for both optimum and suboptimum detectors (* ≡ opt., (-) ≡ sub-opt.), and where the particular

signal and noise structures are specifically introduced. Examples of the latter calculations are given in Sec. 7.5 ff. Figures 7.3, 7.4 show typical curves for $(p_D^*/2)$ $(\equiv P_D^*/p)$ and $P_e^{(*)}$, respectively. Binary as well as the "on-off" signal cases are included. As expected, decreasing the false alarm probability $(\alpha_F^{(*)})$ increases the magnitude of $\sigma_{on}^{(*)}$ needed to obtain a given $P_D^{(*)}$.

Another set of canonical relations are the probability controls, $C_{N.P.}^{(*)}$; $C_{I.O.}^{(*)}$, cf. (6.11), (6.21a), (6.27) etc., which appear in the various expressions for the minimum detectable signals (Sec. 6.2 et seq.). These are

$$C_{N.P.}^{(*)} \equiv \Theta^{-1}(2p_D^{(*)}-1)+\Theta^{-1}(1-2\alpha_F^{(*)}) \; ; \; C_{I.O.}^{(*)} \equiv 2\Theta^{-1}(1-2P_e^*) \; , \tag{7.14}$$

respectively for the Neyman-Pearson and Ideal Observers. Figures 7.5, 7.6 illustrate these quantities.

II. "Basic Ingredients":

These are the various non-linear statistics of the accompanying (non-gaussian + gauss) noise, which are particular elements of the processing gains $(\Pi^{(*)})$, minimum detectable signals, $\sigma_{on}^{(*)}$, etc. and bounds on the acceptable size of the input signals $(a_o^2 << 1)$. From (A.2-42a) we have specifically

$$L^{(2)} \equiv \left\langle \left(\frac{w_1'}{w_1}\right)^2 \right\rangle_o = \left\langle \ell^2 \right\rangle_o = \int_{-\infty}^{\infty} \ell^2 w_1(x)dx \; (>0); \; \ell \equiv \frac{d}{dx} \log w_1(x), \text{ etc.}; \tag{7.15a}$$

$$L^{(4)} \equiv \left\langle \left(\frac{w_1''}{w_1}\right)^2 \right\rangle_o = \left\langle (\ell'+\ell^2)^2 \right\rangle_o = \int_{-\infty}^{\infty} (\ell'+\ell^2)^2 w_1(x)dx \; (>0), \tag{7.15b}$$

$$L^{(2,2)} \equiv 2\left\langle \left(\frac{w_1'}{w_1}\right)^4 \right\rangle_o = 2\left\langle \ell^4 \right\rangle_o = 2\int_{-\infty}^{\infty} \ell^4 w_1(x)dx \; (>0), \tag{7.15c}$$

$$L^{(6)} \equiv \left\langle \left(\frac{w_1''}{w_1}\right)^3 \right\rangle_o = \left\langle (\ell'+\ell^2)^3 \right\rangle_o = \int_{-\infty}^{\infty} (\ell'+\ell^2)^3 w_1(x)dx \; (\gtrless 0). \tag{7.15d}$$

All these quantities are positive, except the last, which for certain noise parameters can be zero or negative. These relations (7.15) hold for Class A, B noise, or for any noise, with pdf $w_{1:E}$, for that matter. Figures 7.7-7.10 show $L^{(2)},\ldots,L^{(6)}$, (7.15a-d), respectively (in db), for strictly and approximately canonical Class A noise,* cf. (3.13). Similarly, Figures 7.11-7.14 give $L^{(2)},\ldots,L^{(6)}$ for the Class B noise of (3.15), (7.11) above (in db) for various $\alpha[=(2-\mu)/\gamma]$, as a function of $\hat{A}_\alpha$.

In the Class A cases these "elements" all approach their gaussian limits as $A_A\to\infty$, viz:

$$\underline{\text{(gauss):}}\quad L^{(2)}=1\ ;\ L^{(4)}=2;\ L^{(2,2)}=6\ ;\ L^{(6)}=8\ ,\ \text{cf. (A.1-22a)}. \tag{7.16}$$

For the Class B noise, we have the results of Figures 7.11-7.14, for example. Of course, when A_B ($\sim \hat{A}_\alpha$, cf. (3.16c))$\to\infty$, we have again gaussian noise, so that (7.16) applies here equally well in the limit. See Sec. 7.5 for further comments on Figs. 7.3-7.14.

---

* Preliminary calculations show that these results are not appreciably different when quasi-canonical Class A noise is used, with $\alpha_0^2<<1$, cf. (3.14) et seq. A complete investigation of this phenomenon, however, remains to be carried out.

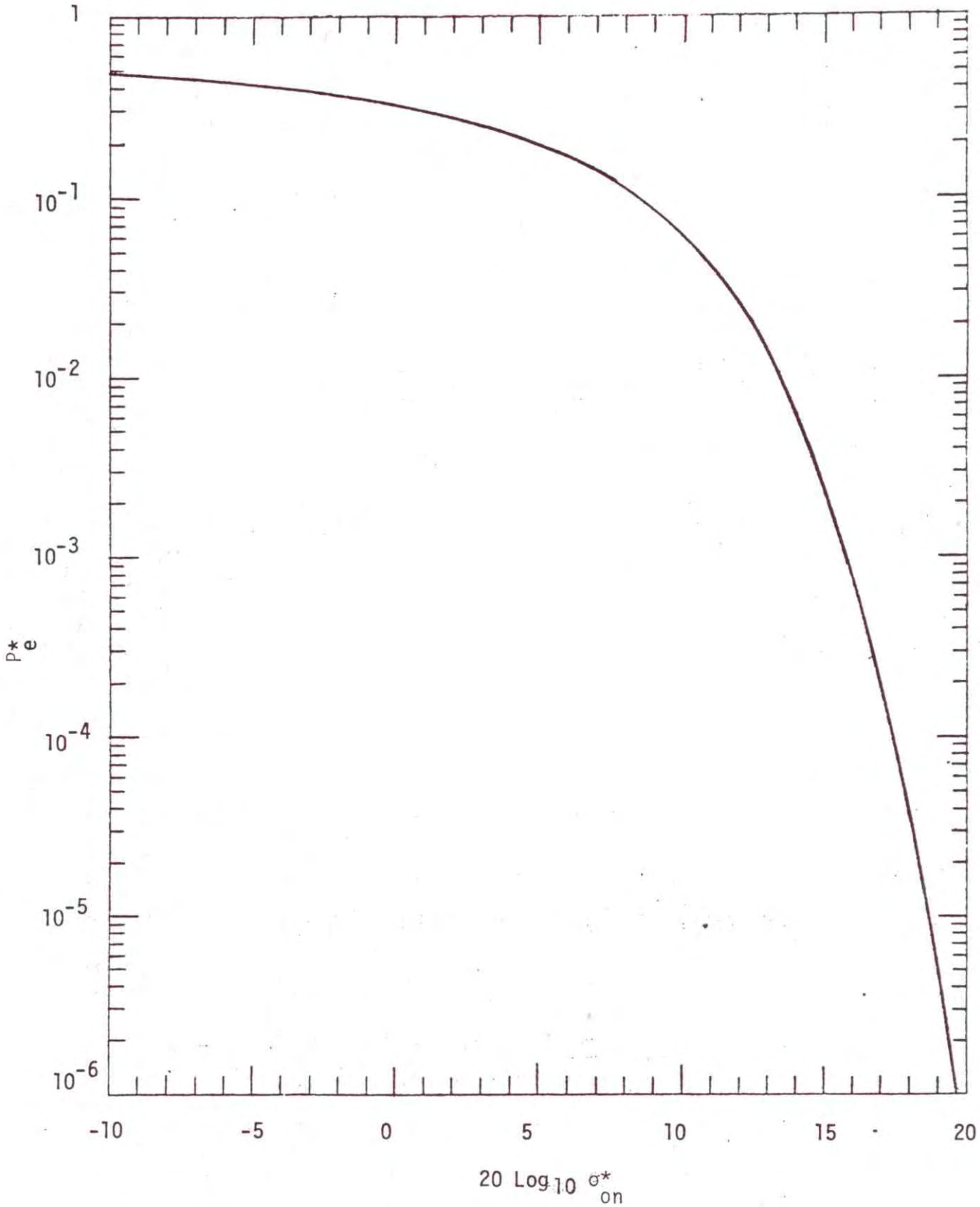

Figure 7.3. Probability of binary error, P_e^*, as canonical function of the variance σ^{*2}_{on}, Eq. (7.13).

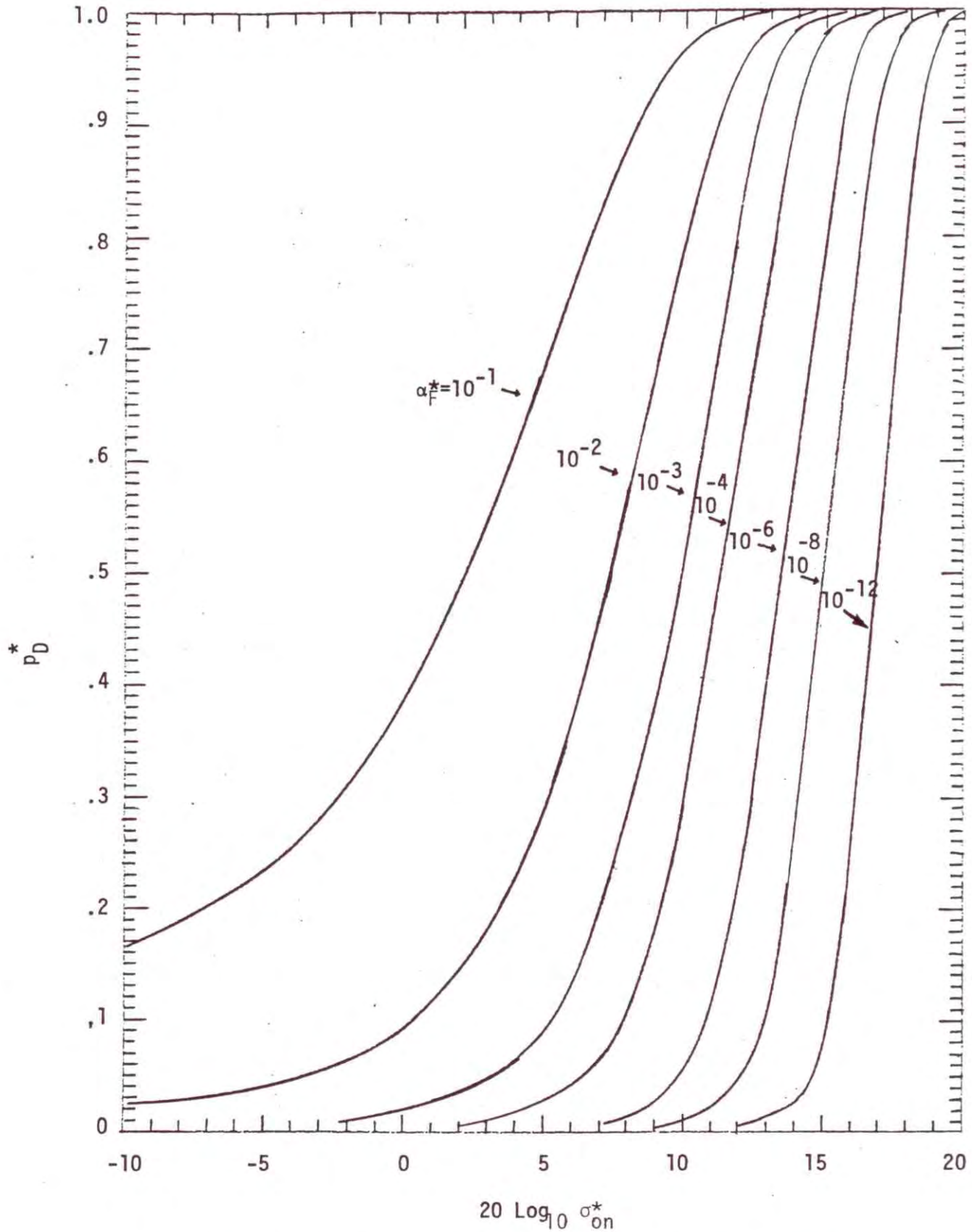

Figure 7.4. Probability of detection, p_D^*, as canonical function of the variance σ_{on}^{*2}, Eq. (7.13).

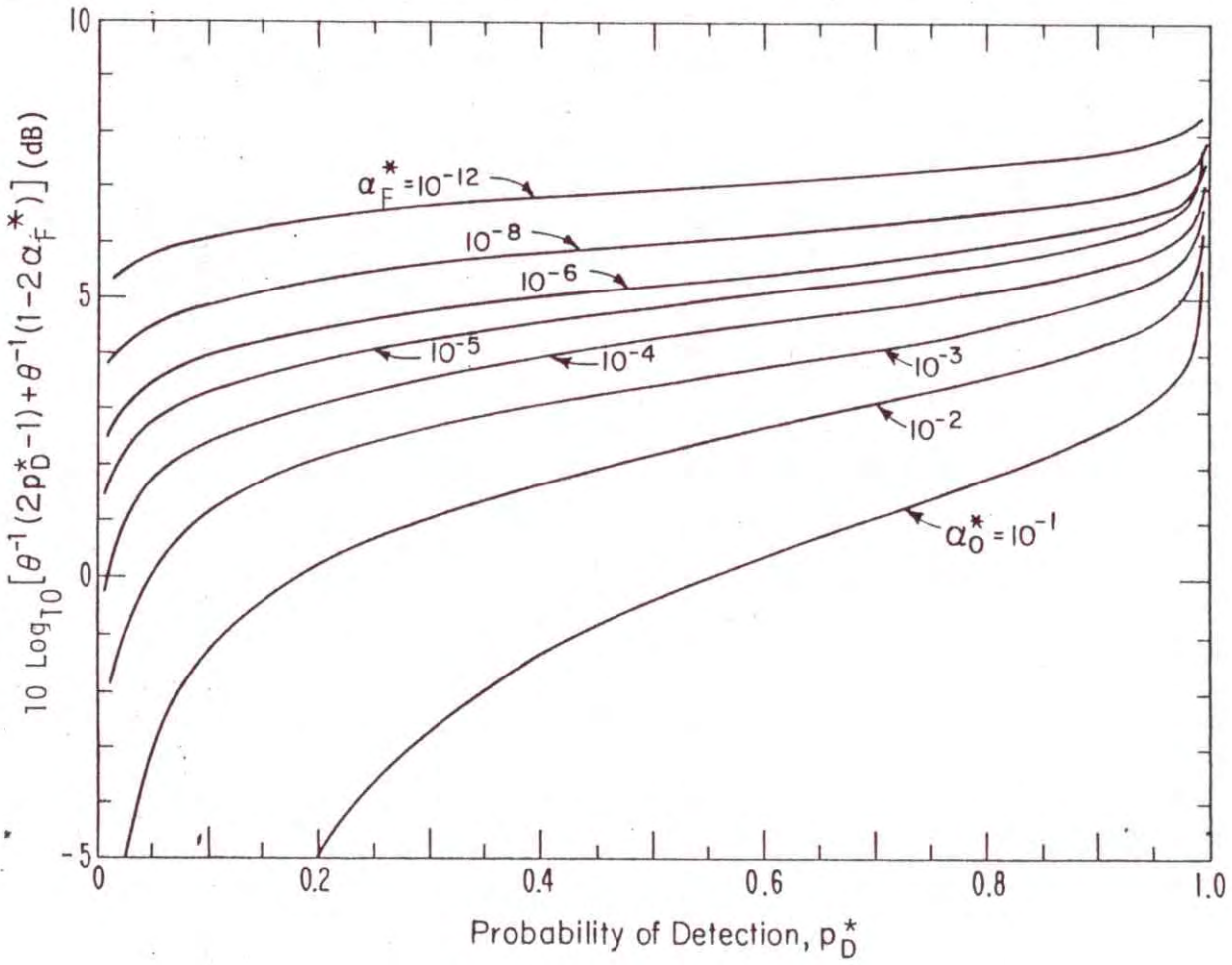

Figure 7.5. Probabilistic controls on detection, C_{NP}^* vs p_D^* ($=P_{D/P}^*$) probabilities of false alarm, α_F^*, Eq. (7.14).

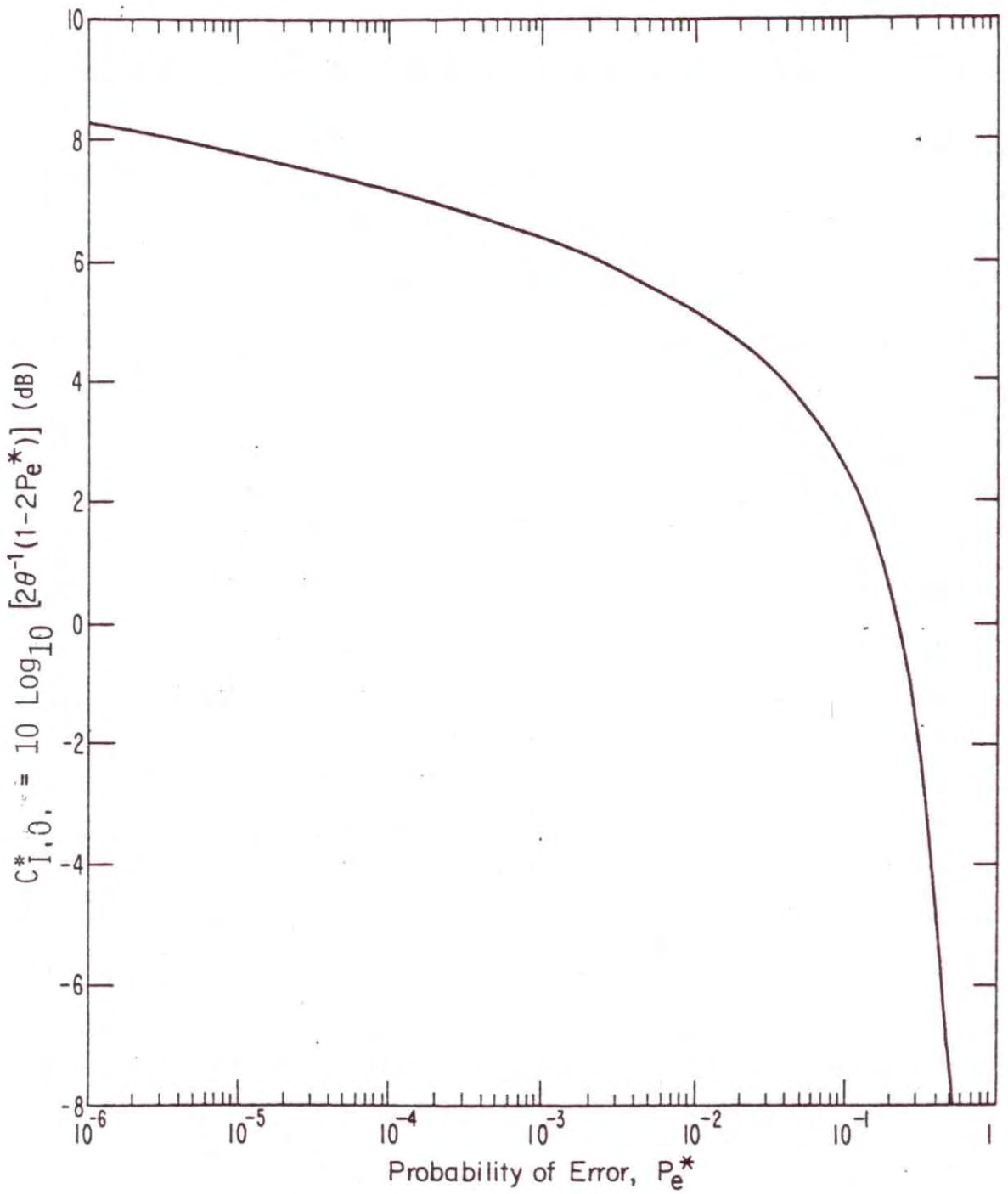

Figure 7.6. Probabilistic controls on detection, $C^*_{I.O.}$ VS P^*_e, Eq (7.14).

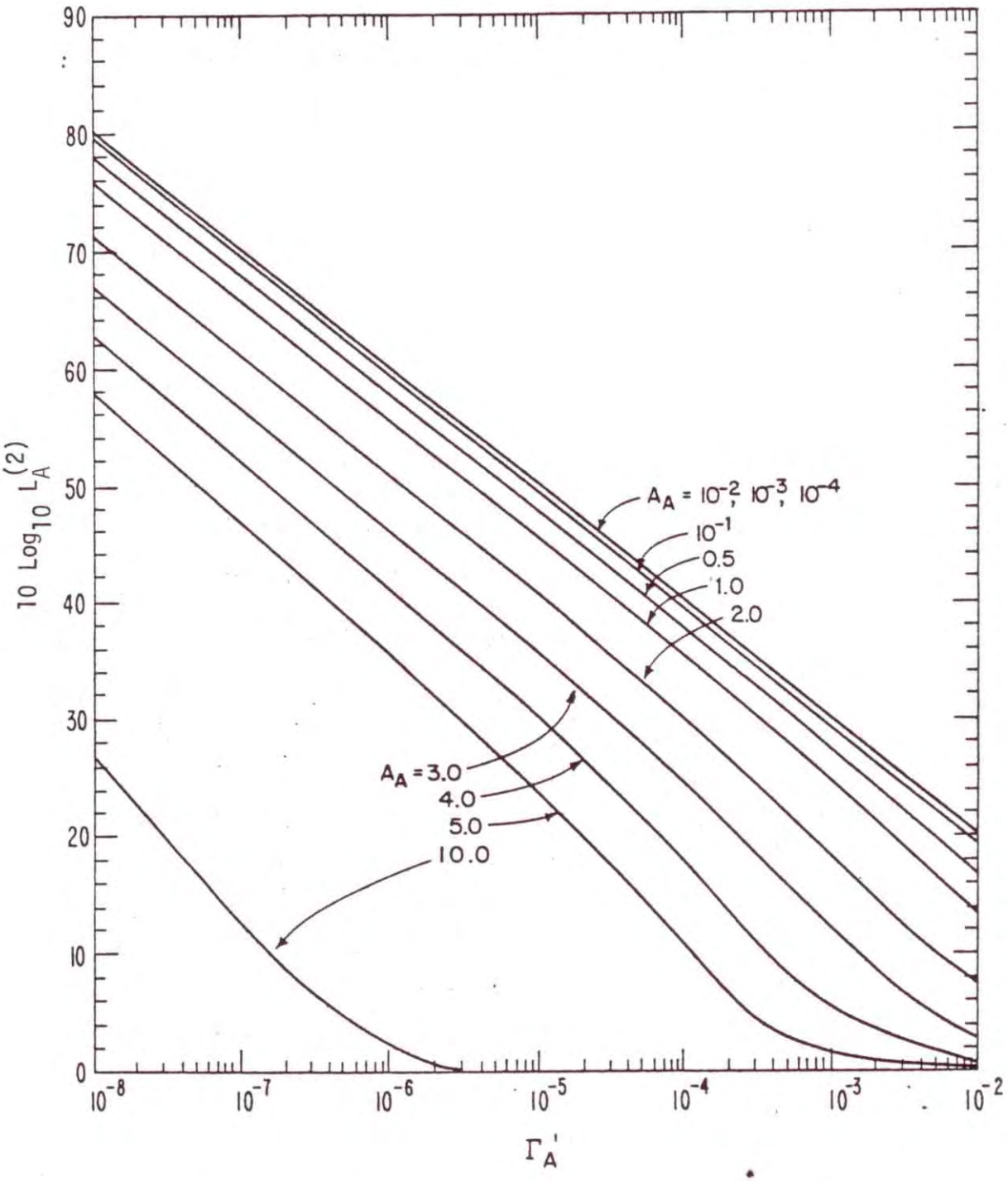

Figure 7.7. Processing gain (Π^*_{coh}/n) per sample, in dB, for optimum coherent threshold detection in Class A EMI, Eq. (7.15a).

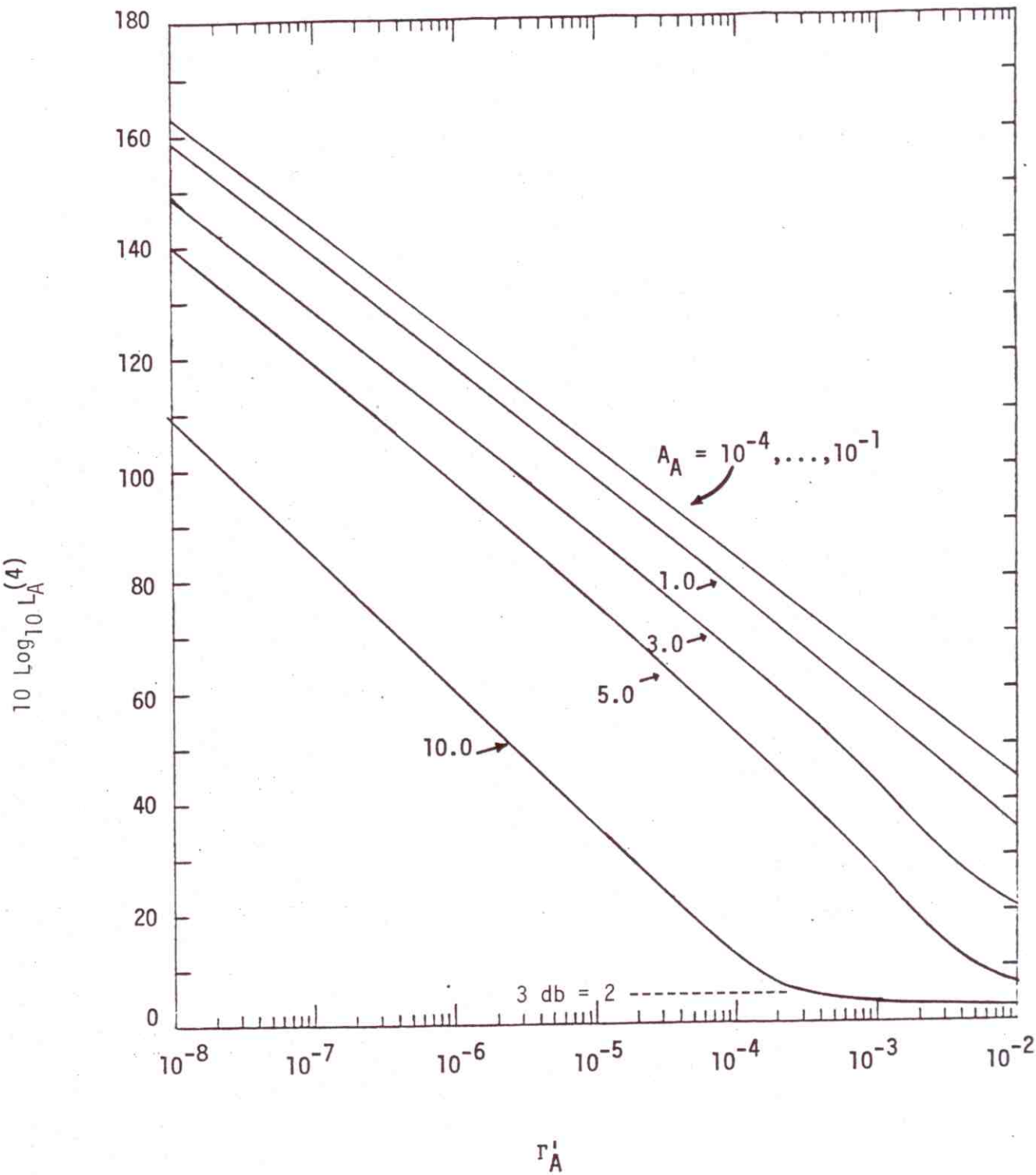

Figure 7.8. $L^{(4)}$ $(=\langle(\ell' + \ell^2)^2\rangle_o)$, in dB, for Class A EMI, Eq. (7.15b).

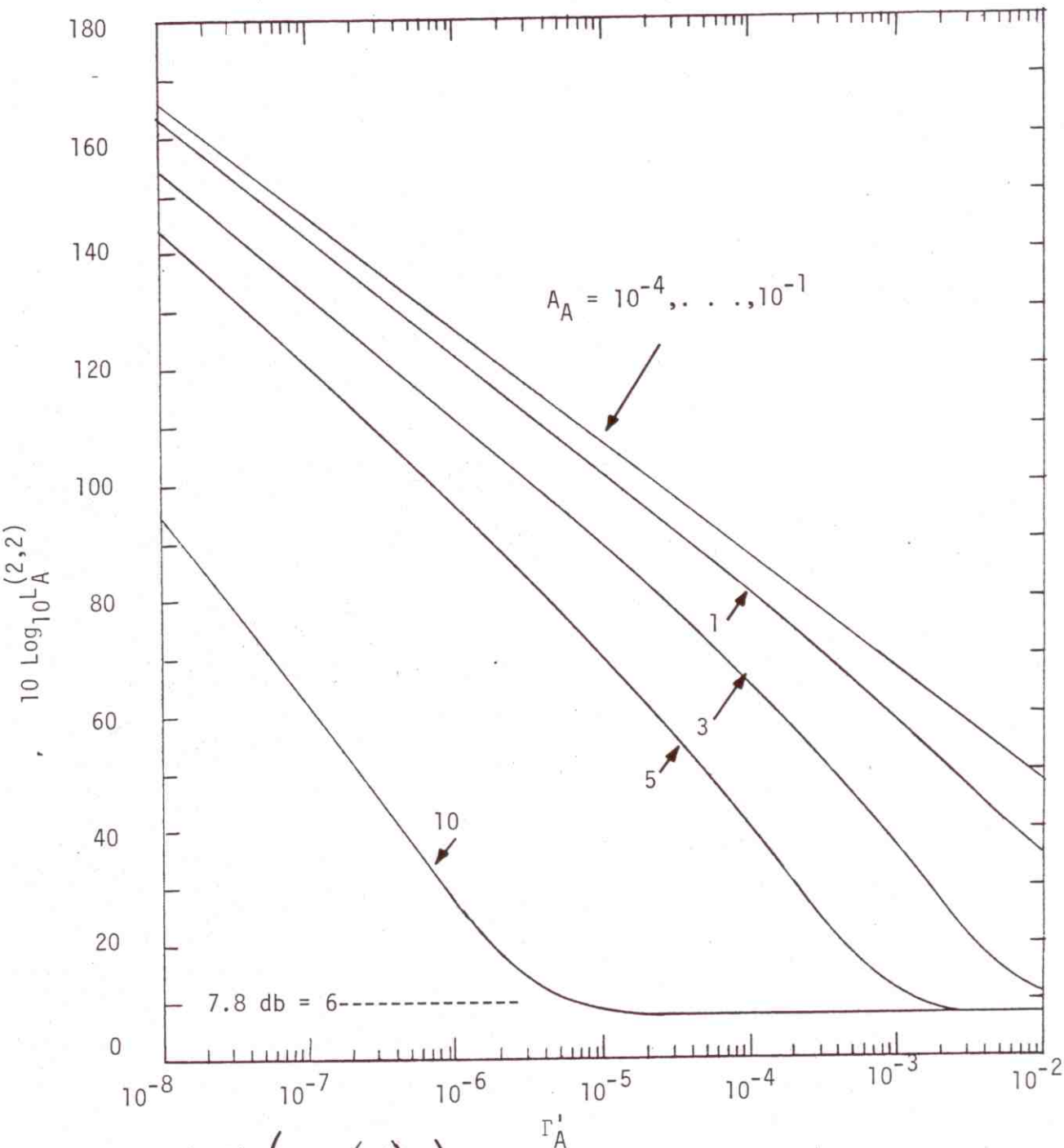

Figure 7.9. $L^{(2,2)}\left(= 2\left\langle \ell^4 \right\rangle_0\right)$ in dB, for Class A EMI, Eq. (7.15c).

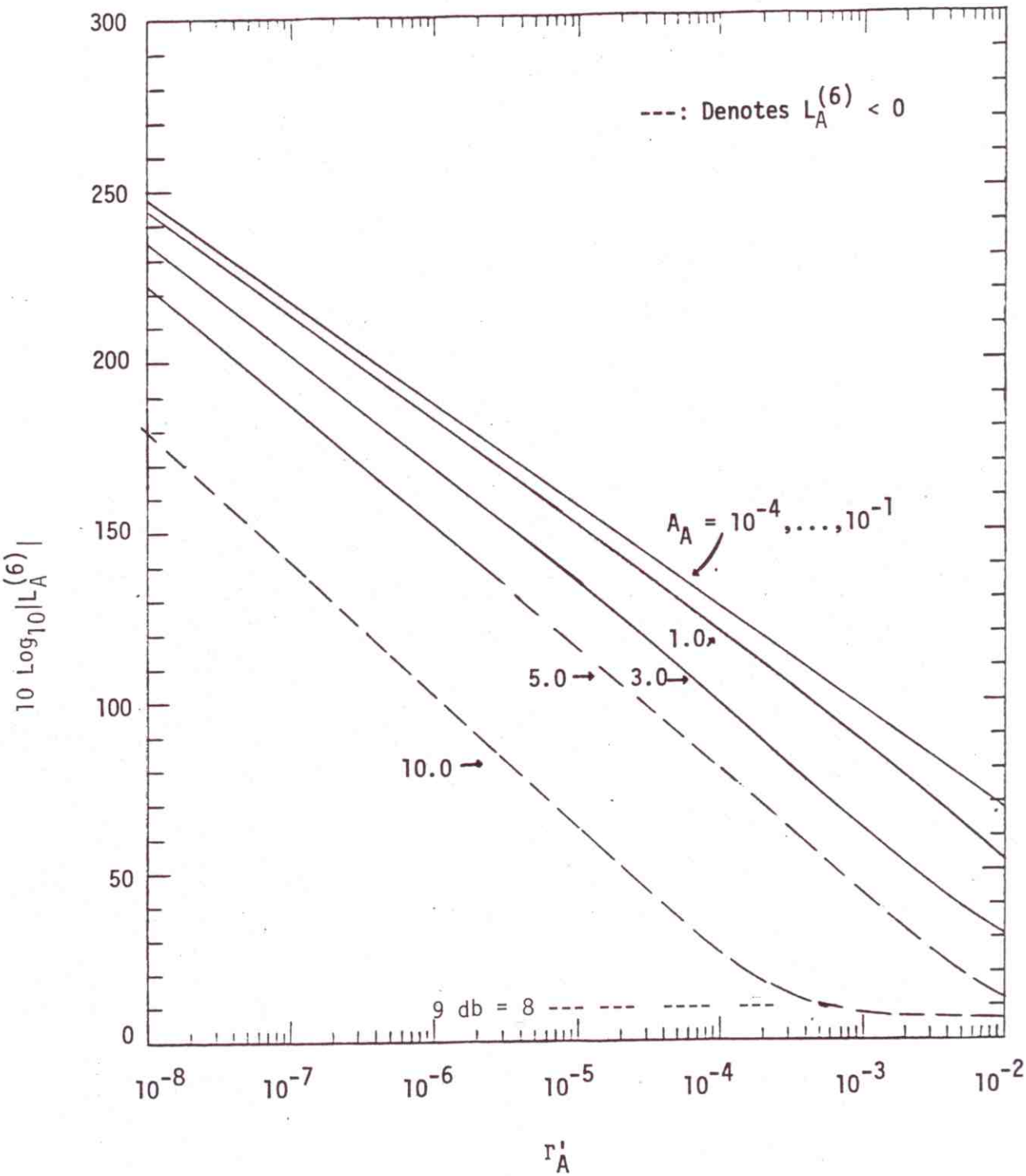

Figure 7.10. $L_A^{(6)}$ $(=\langle(\ell' + \ell^2)^3\rangle_o)$, magnitude in dB, for Class A EMI, Eq. (7.15d).

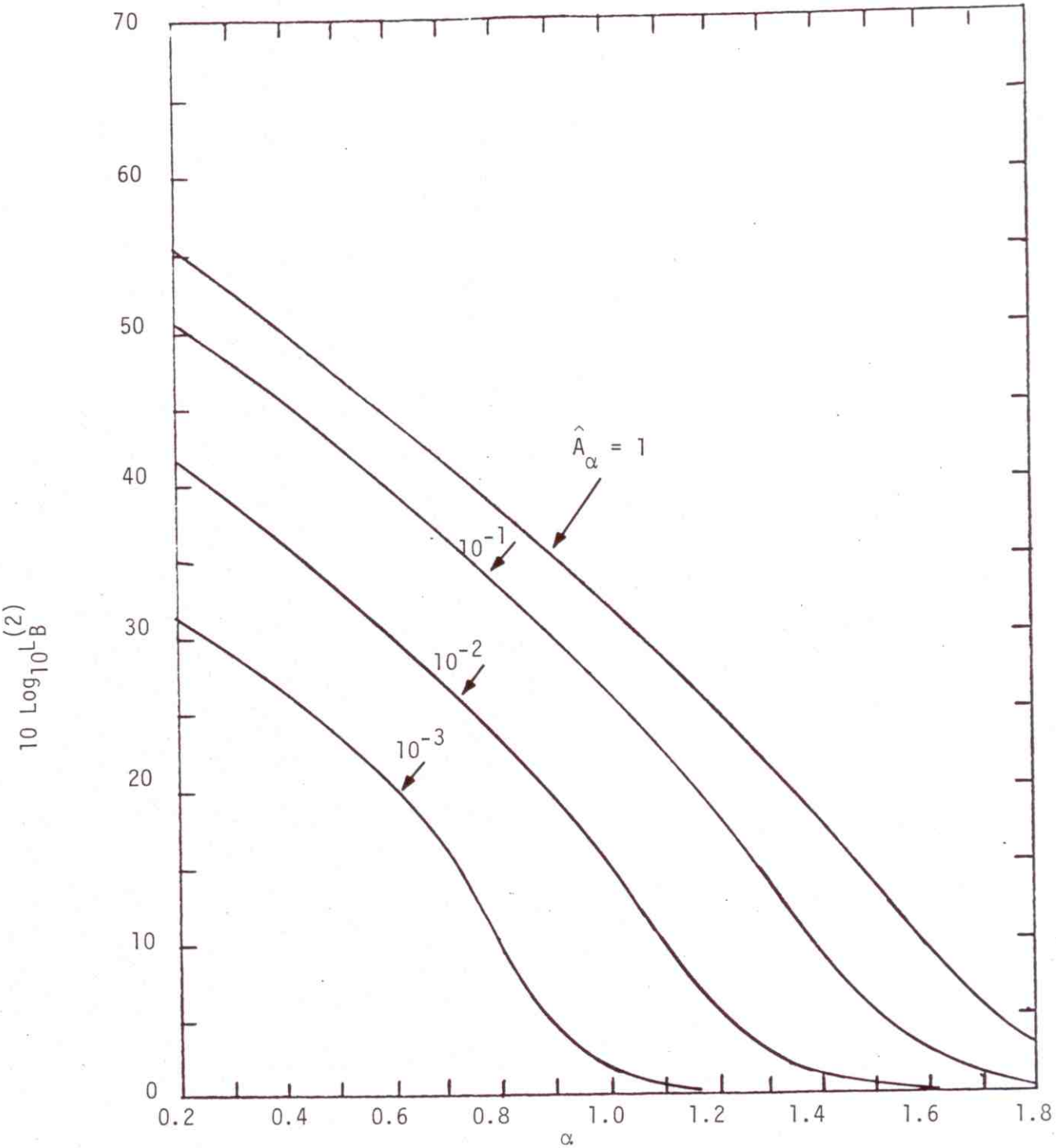

Figure 7.11. Processing gain (Π^*_{coh}/n) per sample, $L_B^{(2)}$, in dB, for optimum coherent threshold detection in Class B EMI, Eq. (7.15a).

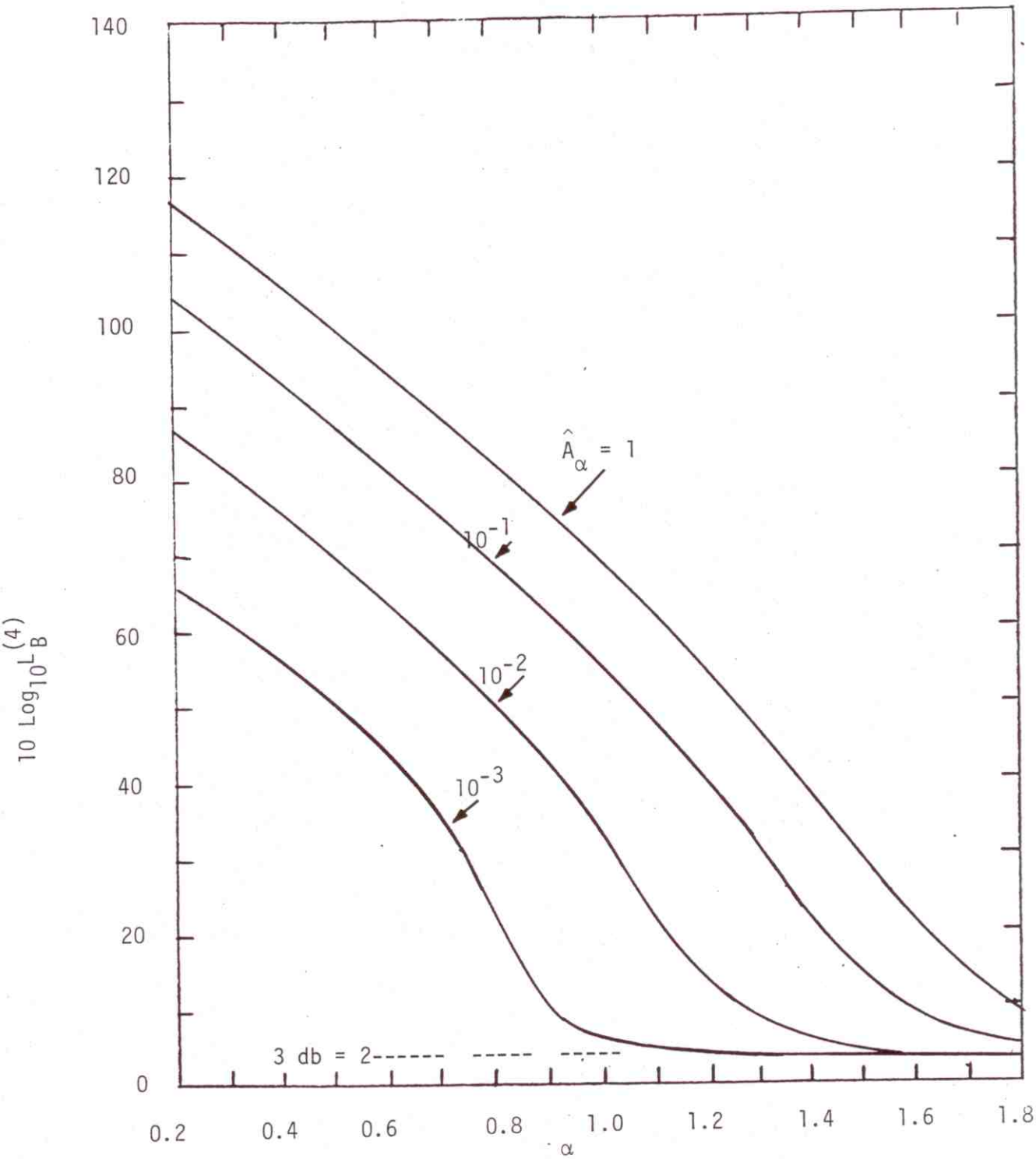

Figure 7.12. $L_B^{(4)}$ $\left(= \left\langle (\ell' + \ell^2)^2 \right\rangle_o \right)$, in dB, for Class B EMI, Eq. (7.15b).

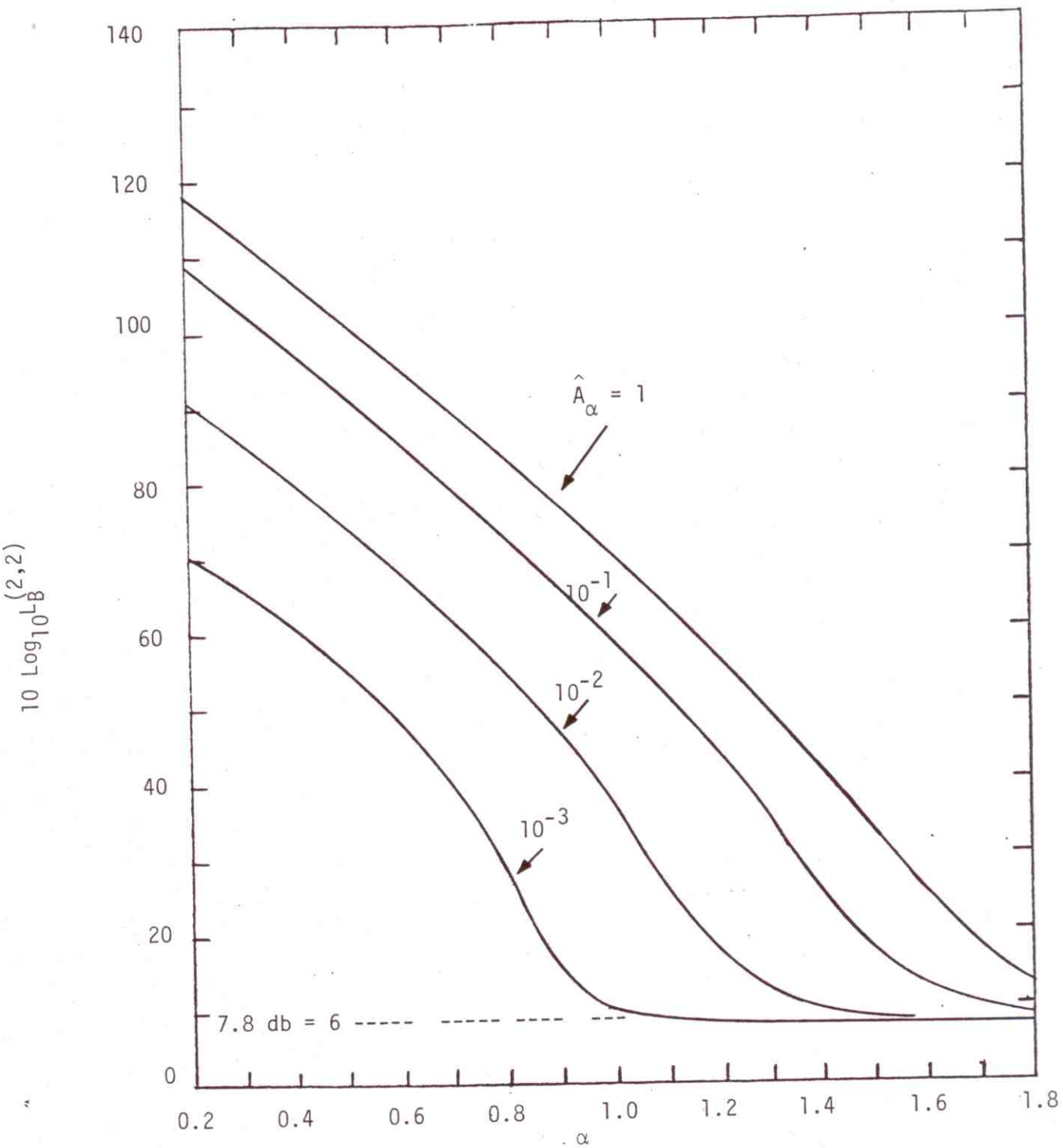

Figure 7.13. $L_B^{(2,2)} \left(= 2\langle \ell^4 \rangle_o \right)$, in dB, for Class B EMI, Eq. (7.15c).

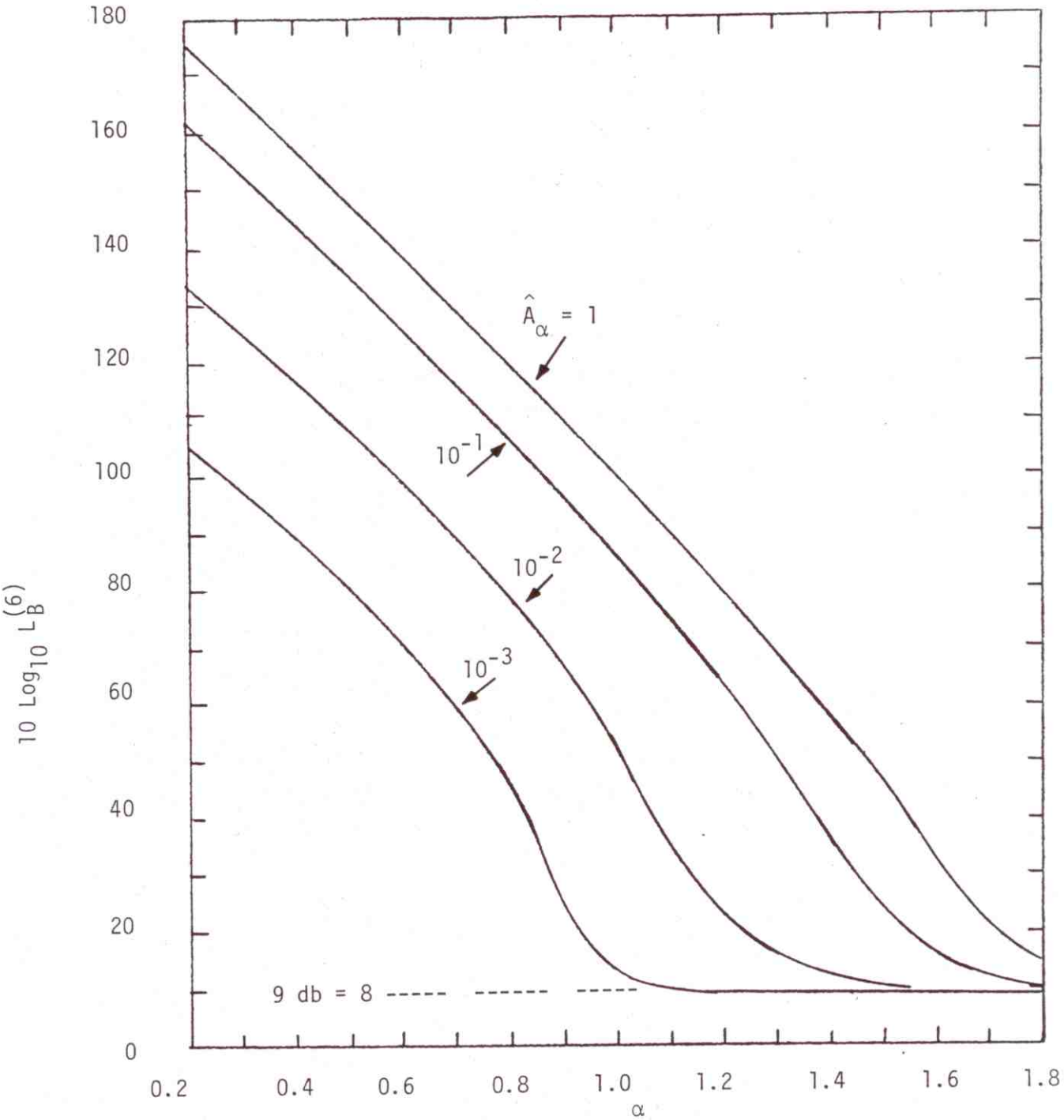

Figure 7.14. $L_B^{(6)}$ $\left(= \left\langle \left(\ell' + \ell^2 \right)^3 \right\rangle_o \right)$, in dB, for Class B EMI, Eq. (7.15d).

III. Processing Gains/per Sample:

The processing gain per sample, $\Pi^{(*)}/n$, are also needed in the evaluation of (optimum) performance. From (6.10), (6.13); (6.24), (6.33) we can write [cf. Tables 6.1a, 6.1b]:

$$\Pi^{*}_{coh/n} = L^{(2)} = \Pi^{(21)*}_{coh}/n \ ;$$

$$\Pi^{*}_{inc}/n = \frac{1}{8}\{L^{(4)}+2L^{(2)^2}(Q_n-1)\}, = \frac{L^{(4)}}{8}, \ (Q_n=1\text{:incoh.signal structure})$$

$$\tilde{=} \ nL^{(2)^2}/8 \ , \ (Q_n = \frac{n}{2} \ (>>1);$$

sinusoids; Eq. (A.2-42e))

(7.17a)

(binary symmetric):

$$\Pi^{(21)*}_{inc} = \frac{L^{(2)^2}}{4}(\hat{Q}^{(21)}_n-1) = 0, \qquad (\hat{Q}^{(21)}_n=1\text{: incoherent structure})$$

$$\tilde{=} \ nL^{(2)^2}/4, \ (\hat{Q}^{(21)}_n=n(>>1),$$

sinusoids, Eq. (A.2-61a)

(7.17b)

explicitly for no, or slow-fading, e.g. $m_{ij}=1$, cf. (7.4a,b) above, and binary symmetric channels, when indicated. We also note from (6.14), (6.15) that in the coherent cases the minimum detectable signal $\langle a_o^2\rangle^{(21)*}_{min\text{-}coh}$ is increased vis-à-vis that of the "on-off" cases; by a factor 4 for orthogonal signals (7.3) and by a factor 2 for antipodal signals, (7.2), according to the definition (6.13), while the processing gain ($\Pi^{(21)*}_{coh}$) remains unchanged. On the

other hand, for incoherent detection, $\langle a_o^2\rangle^{(21)*}_{\text{min-inc}} \equiv \overline{a_o^2}$, (a_o^2), (symmetrical channels), cf. (6.33), and the processing gain is increased vis-à-vis the "on-off" cases by a factor 2 to the extent that the binary signals have coherent waveform structures, cf. (7.17b) vs. (7.17a), n>>1. Figures 7.7, 7.11 show $\Pi^*_{\text{coh/n}}$ (db) for Class A and B noise respectively in the coherent cases. Figures 7.8, 7.12 show $(\Pi^*_{\text{inc/n}})$ (db) + 9.0 db (= 10 $\log_{10}$ 8), also for Class A and B noise, when Q_n = 1 for the "on-off" cases. Figures 7.15, 7.16 illustrate $\Pi^*_{\text{inc/n}}$ for Q_n = 10, Class A and Class B noise respectively. The limiting cases (n>>1, coherent signal structure) are readily calculated form (7.17a,b) with the help of the data of Figs. 7.7, 7.11. Generally, as the noise becomes more gaussian, these processing gains approach their gaussian limits (as expected) where now $L^{(2)}\to 1$, $L^{(4)}\to 2$. (See Sec. 7.5 for comments on Figs. 7.15, 7.16.)

IV. The Optimum H_o- Variances σ^{*2}_{on} :

These quantities, σ^{*2}_{on}, appear as the argument of the probabilistic performance measures, P^*_D, P^*_e, cf. (7.13), and are consequently a principal goal of our computations. Specifically, from Tables 6.1a,b we can write in summary:

A. Coherent Detection:

$$\left.\begin{array}{l|l} \sigma^{*2}_{\text{on-coh}} = \bar{a}_o^2 nL^{(2)} & \equiv 2\langle a_o^2\rangle^*_{\text{min-coh}}\Pi^*_{\text{coh}}, \text{ [Eq.(6.9)],"on-off" signals} \\ \left\{ \begin{array}{l} (\sigma^{(21)*}_{\text{on-coh}})^2 = 2\bar{a}_o^2 nL^{(2)} \\ \quad " \qquad\quad = 4\bar{a}_o^2 nL^{(2)} \end{array} \right. & \begin{array}{l} \text{: orthogonal signals, [Eq. (6.15b)]} \\ \text{: antipodal signals, [Eq. (6.15a)] ,} \end{array} \end{array}\right\} \quad (7.18)$$

these last for symmetrical channels ($a_o^{(1)} = a_o^{(2)} = a_o$), ($p_1 = p_2 = 1/2$), and no or stationary fading small or large, rapid or slow ($\bar{a}_o = a_o$, $\bar{a}_{oi} = \bar{a}_o$), all n ($\geq$ 1).

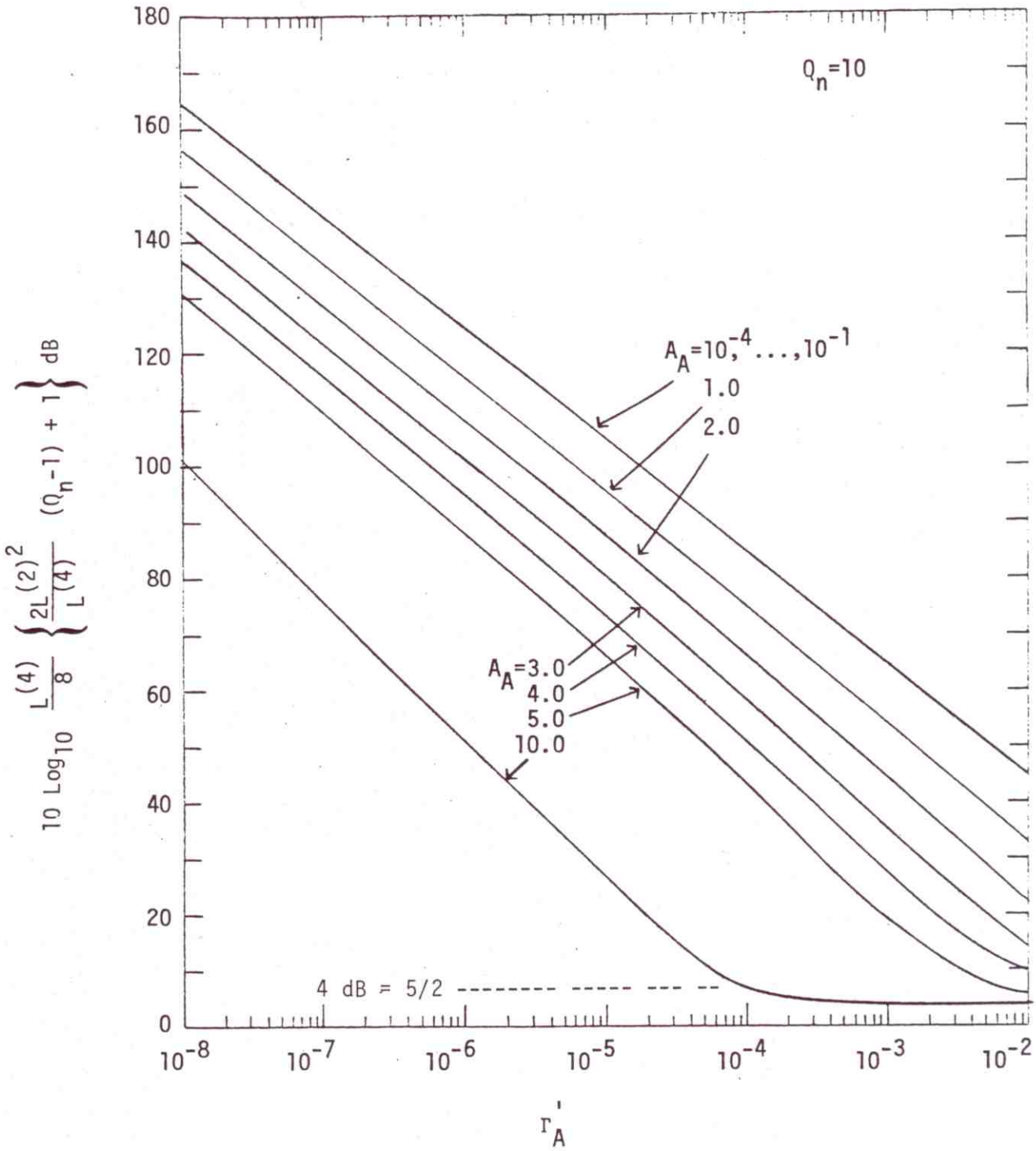

Figure 7.15. Processing gain (Π^*_{inc}/n) per sample, in dB, for optimum incoherent threshold detection in Class A EMI, for signals with partially incoherent structure (Q_n=10), Eq. (7.17a).

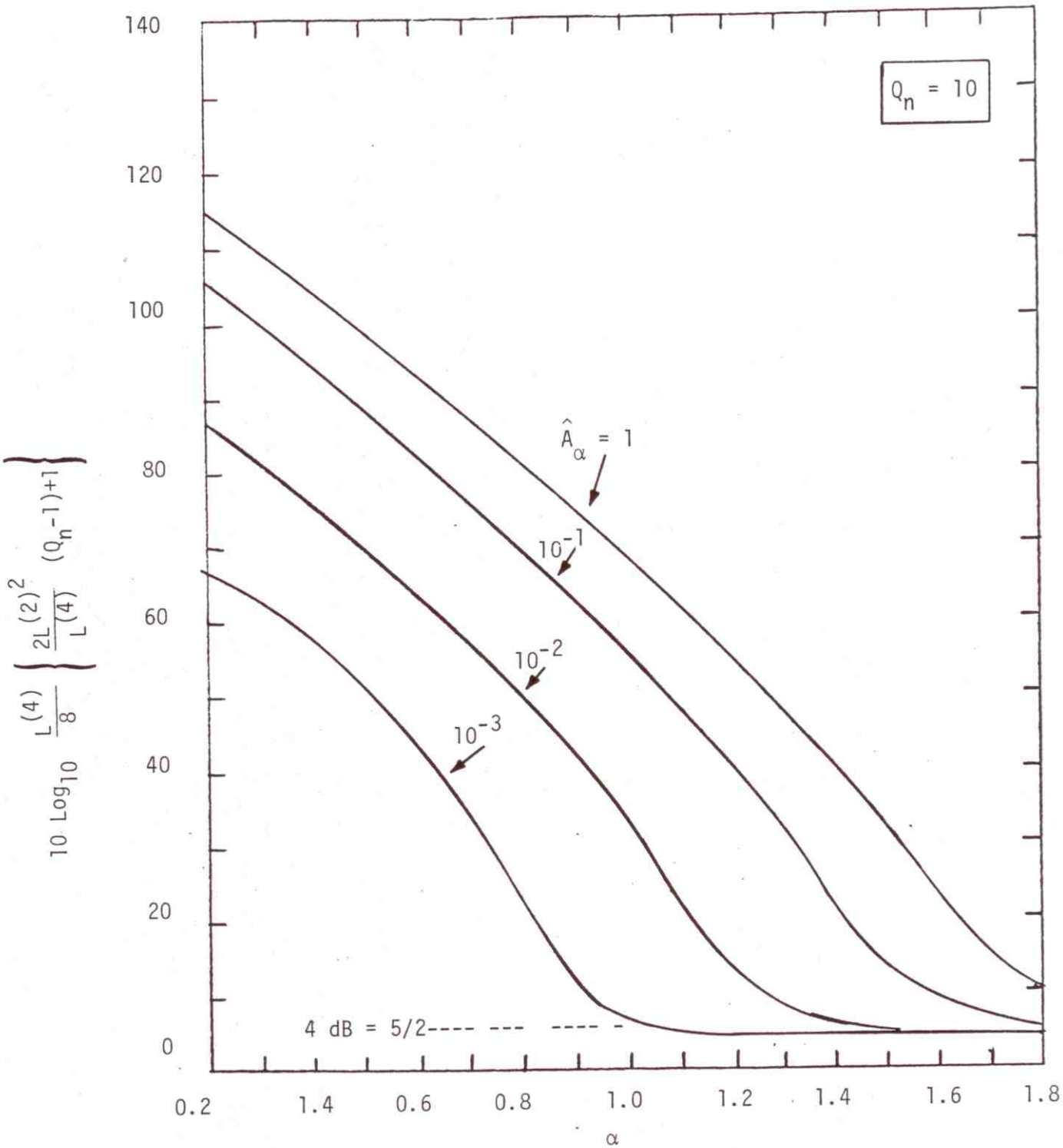

Figure 7.16. Processing gain (Π^*_{inc}/n) per sample, in dB, for optimum incoherent threshold detection in Class B EMI, for signals with partially incoherent structure ($Q_n = 10$), Eq. (7.17a).

B. Incoherent Detection:

$$\sigma^{*2}_{\text{on-inc}} = \frac{\overline{a_o^2}}{4}\, n\{L^{(4)} \pm 2L^{(2)^2}(Q_n - 1)\} \equiv 2\langle a_o^2\rangle^{*2}_{\text{min-inc}}\Pi^{*}_{\text{inc}} : \underline{\text{"on-off"}} \tag{7.19a}$$

$$\sigma^{*(21)^2}_{\text{on-inc}} = \frac{\overline{a_o^2}\, nL^{(2)^2}}{2}\,(\hat{Q}_n^{(21)} - 1) \equiv 2(\langle a_o^2\rangle^{(21)*}_{\text{min-inc}})^2\Pi^{(21)*}_{\text{inc}} : \left.\begin{array}{l}\\ \\ \underline{\text{binary symmetrical}}\ ,\end{array}\right\} \tag{7.19b}$$

where $m_{ij} = 1$, $a_o^{(2)} = a_o^{(2)} = a_o$, etc., now for slow or no fading, which is more restricted than the above, (7.18). Here we have

$$Q_n - 1 \equiv \frac{1}{n}\sum_{ij}^{n}{}' \rho_{ij}^2 \quad ; \quad \hat{Q}_n^{(21)} - 1 \equiv \frac{1}{n}\sum_{ij}^{n}{}' [\rho_{ij}^{(2)} = \rho_{ij}^{(1)}]^2,\ n \geq 1, \tag{7.19c}$$

cf. (6.25), (6.33), (6.33a), and Table 6.1b. Special results are

$$\left.\begin{array}{l}\text{(i). } \underline{\text{incoherent signal structure:}} \\ \qquad (\sigma^{*}_{\text{on-inc}})^2 = \overline{a_o^2}\, nL^{(4)}/4\ , \quad (n \geq 1) \\ \text{(iii). } \underline{\text{coherent (sinusoidal) signal structure:}} \\ \qquad (\sigma^{*}_{\text{on-inc}})^2 = \overline{a_o^2}\, n^2 L^{(2)^2}/4,\ [Q_n \tilde{=} \tfrac{n}{2}]\ (n \gg 1)\end{array}\right\} : \underline{\text{"on-off" signals}}\ , \tag{7.20a}$$

and in the case of the binary symmetric channel above, these are [cf. (7.17a,b) in (7.19a,b)]

(i). incoherent signal structure:

$$(\sigma^{*(21)}_{\text{on-inc}})^2 = 0: \text{ [detection of two equal energy signals: no distinction between } H_1 \text{ and } H_2.]$$

(ii). coherent (sinusoidal) signal structure:

$$(\sigma^{*(21)}_{\text{on-inc}})^2 = \overline{a_o^2}\, n^2 L(2)^2/2 \ , \ [\hat{Q}_n^{(21)} - 1 \cong n \ (>>1)].$$

} "binary signals" (7.20b)

The advantage of operation with coherent signal structures in the incoherent, "on-off" mode of detection vis-à-vis incoherent signal structures is at once apparent from (7.20a):

$$\frac{(\sigma^{*}_{\text{on-inc}})^2_{\text{coh st.}}}{(\sigma^{*}_{\text{on-inc}})^2_{\text{inch. st.}}} = \frac{nL(2)^2}{L^{(4)}} \ (>>1), \ (n>>1) \ . \qquad (7.21)$$

Although $1>L^{(2)^2}/L^{(4)} \geq 0$, $L^{(2)^2} \sim L^{(4)}$ within O(10 db), so that for the customary large values of sample-size n, the advantage of being able to employ coherent signal structures, i.e. having channels with little or no doppler spread and/or rapid fading, is essentially $\sim n$, which is considerable where n is at all large, cf. V, Section 6.2 above. With binary (symmetric) signal operation coherent signal structure is critical, cf. (7.20b), if we are to avoid having to distinguish between two essentially equal "energy signals", whose original frequency structures are no longer distinct, because of the time- and frequency "smearing" (i.e. spreading) produced in the channel. Thus, for sufficiently "widely-spread" channels it becomes necessary to employ the "on-off" transmission mode, cf. (7.20a), where now at least, we are required to distinguish a non-vanishing (desired) signal

however distorted, from the condition of noise alone. Quantitatively, the larger the magnitudes of Q_n, $Q_n^{(21)}$, the larger the variance $(\sigma^*_{on})^2$ and the better the detector performance, cf. (7.13).

C. The Composite Detector:

$$\sigma^{*2}_{o\text{-comp}} = \sigma^{*2}_{o\text{-coh}} + \sigma^{*2}_{o\text{-inc}}$$

$$= n\{\bar{a}_o^2 L^{(2)}[\frac{1}{2n}\sum_i \langle s_i\rangle^2] + \frac{1}{4}\overline{a_o^2}\{L^{(4)} + 2L^{(2)^2}[Q_n - 1]\}\}: \quad \underline{\text{"on-off"}} \ . \tag{7.22a}$$

$$(\sigma^{(21)*}_{o\text{-comp}})^2 = n\{\bar{a}_o^2 L^{(2)} \frac{1}{2n}\sum_i [\langle s_i^{(2)}\rangle - \langle s_i^{(1)}\rangle]^2 + \frac{\overline{a_o^2}}{2} L^{(2)^2}(\hat{Q}_n^{(21)} - 1)\} : \quad : \underline{\text{"binary symmetric"}} \ . \tag{7.22b}$$

Here the sum in (7.22b) reduces to (2,4), respectively for completely coherent received orthogonal, or antipodal binary signals, cf. (7.18). The sum in (7.22a) likewise reduces to unity. Again, we assume no or slow fading here, and stationary noise and channel characteristics. Frequently, we do not have full coherence at the receiver, so that $\rho_{ij} = \langle s_i s_j\rangle \neq \bar{s}_i\bar{s}_j$, $(\bar{s}_{i,j} \neq 0)$, and we must use both first- and second-order statistics of the signal, as indicated above. We shall use (7.22) in (7.13) in Section 7.5, when we come to calculate performance.

V. Bounds on Input Signal Size:

The bounds (x_0^*, y_0^*) on the maximum input signal for which $\mathrm{var}_1 g_n^* \doteq \mathrm{var}_0 g_n^*$, required both for the LOBD and AOD character of these optimal threshold detection algorithms, are given in Section 6.3. We summarize the results for the usual conditions (above). We start with the "on-off" signal cases:

A. Coherent Detection:

$$x_0^* = L^{(2)} \Big/ \left(L^{(2,2)} \Big/ 2 - (1-\eta) L^{(2)^2} \right) = \frac{\langle \ell^2 \rangle_0}{\mathrm{var}_0 \ell^2} \tag{7.23}$$

[rapid fading, for no or slow fading, $\eta \sim 0$, Eq. (6.71)].

B. Incoherent Detection:

$$y_0^* \Big|_{\text{incoh.sig.struct.}} = \frac{L^{(4)}}{\left| \frac{L^{(6)}}{2} + 6L^{(2)} L^{(2,2)} \right|};$$

$$y_0^* \Big|_{\text{coh. sig. struct.}} = \frac{L^{(2)}}{3L^{(2,2)} + 2L^{(2)^2}} \quad , \text{[Eqs. (6.72)]}. \tag{7.24}$$

For the binary symmetric channel, with no, slow or rapid, fading, we refer back to Eqs. (6.77), (6.78). Finally, when the composite detector is used [cf. Sec. 6.5], we choose the stricter of the two bounds (x_0^*, y_0^*), usually that for incoherent detection. Figures 7.17-7.19 show (7.23), (7.24) for Class A noise, while Figures 7.20-7.22 give (x_0^*, y_0^*) for various Class B cases.

7.4 Performance Elements for Suboptimum Threshold Detectors:

Just as we have established the "elements" needed to determine the performance of optimum threshold detection systems in Sec. 7.3 above, we can proceed to do the same here for suboptimum systems. As before, we

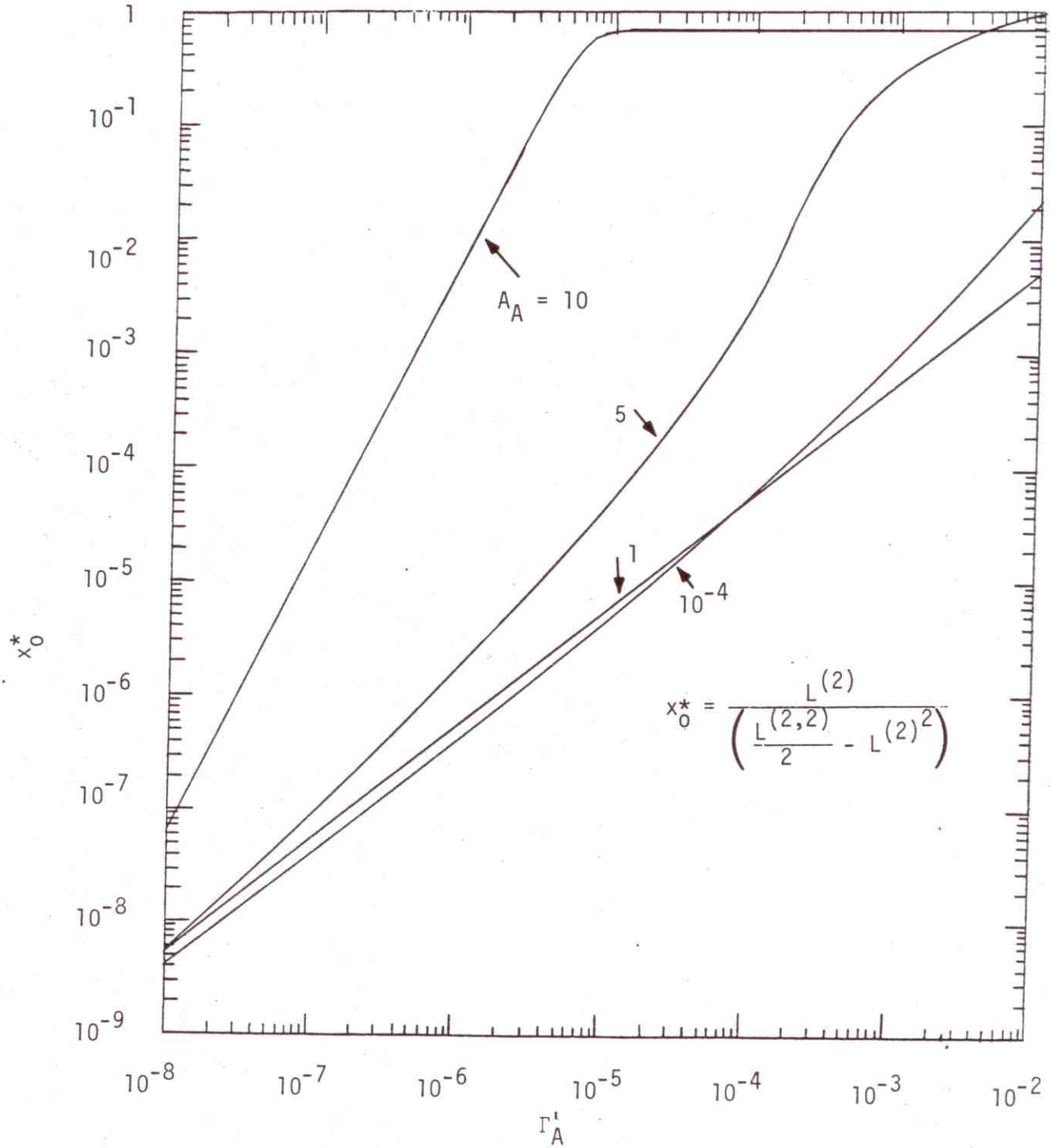

Figure 7.17. The bound, x_o^*, for coherent detection of (coherent) signals in Class A EMI, Eq. (7.23) (No or little fading: $\overline{a_o^2} \doteq \overline{a_o}^2$).

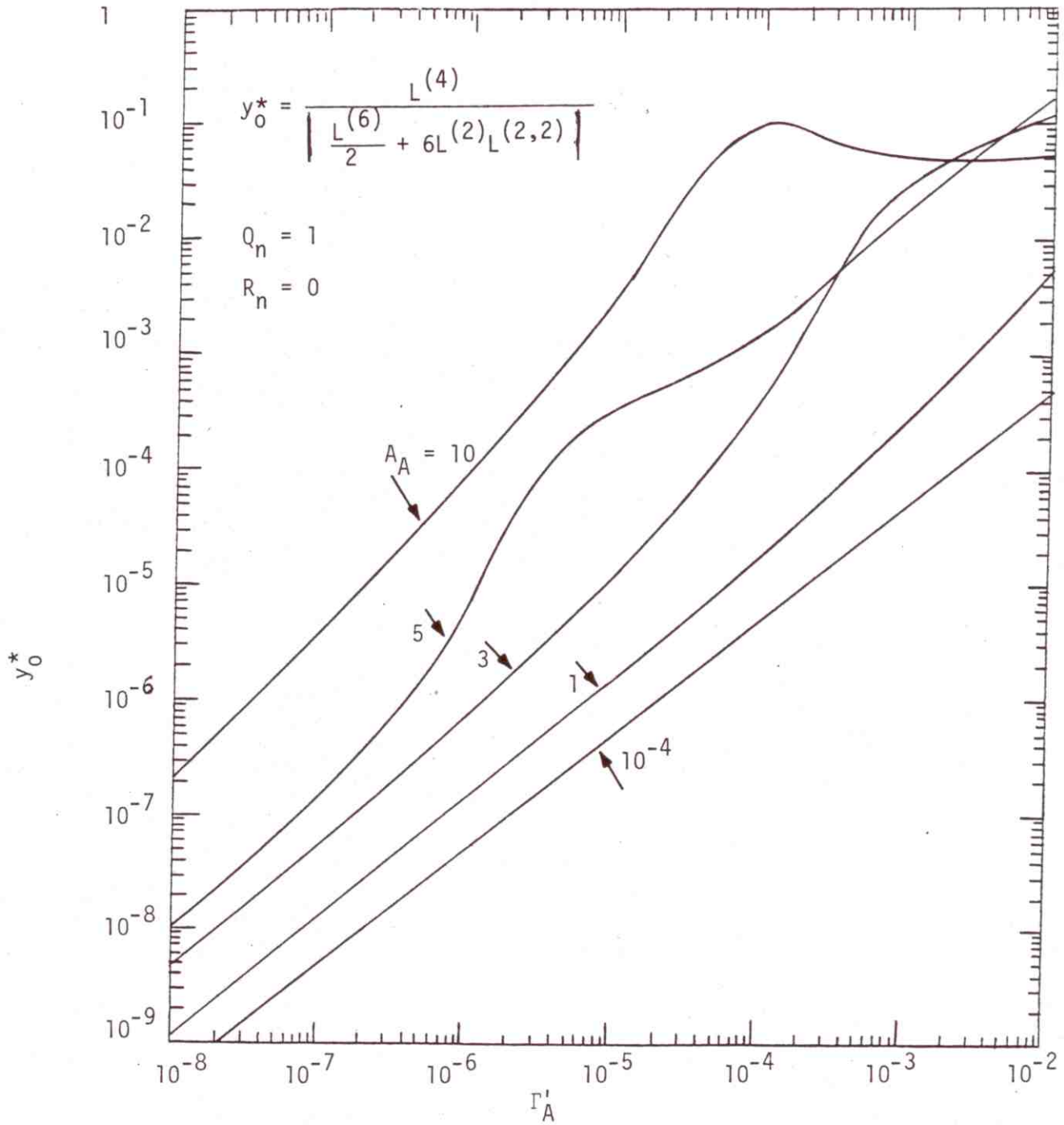

Figure 7.18. The bound, y_o^*, for incoherent detection of signals with fully incoherent structure in Class A EMI ($Q_n = 1$, $R_n = 0$), Eq. (7.24), arbitrary fading.

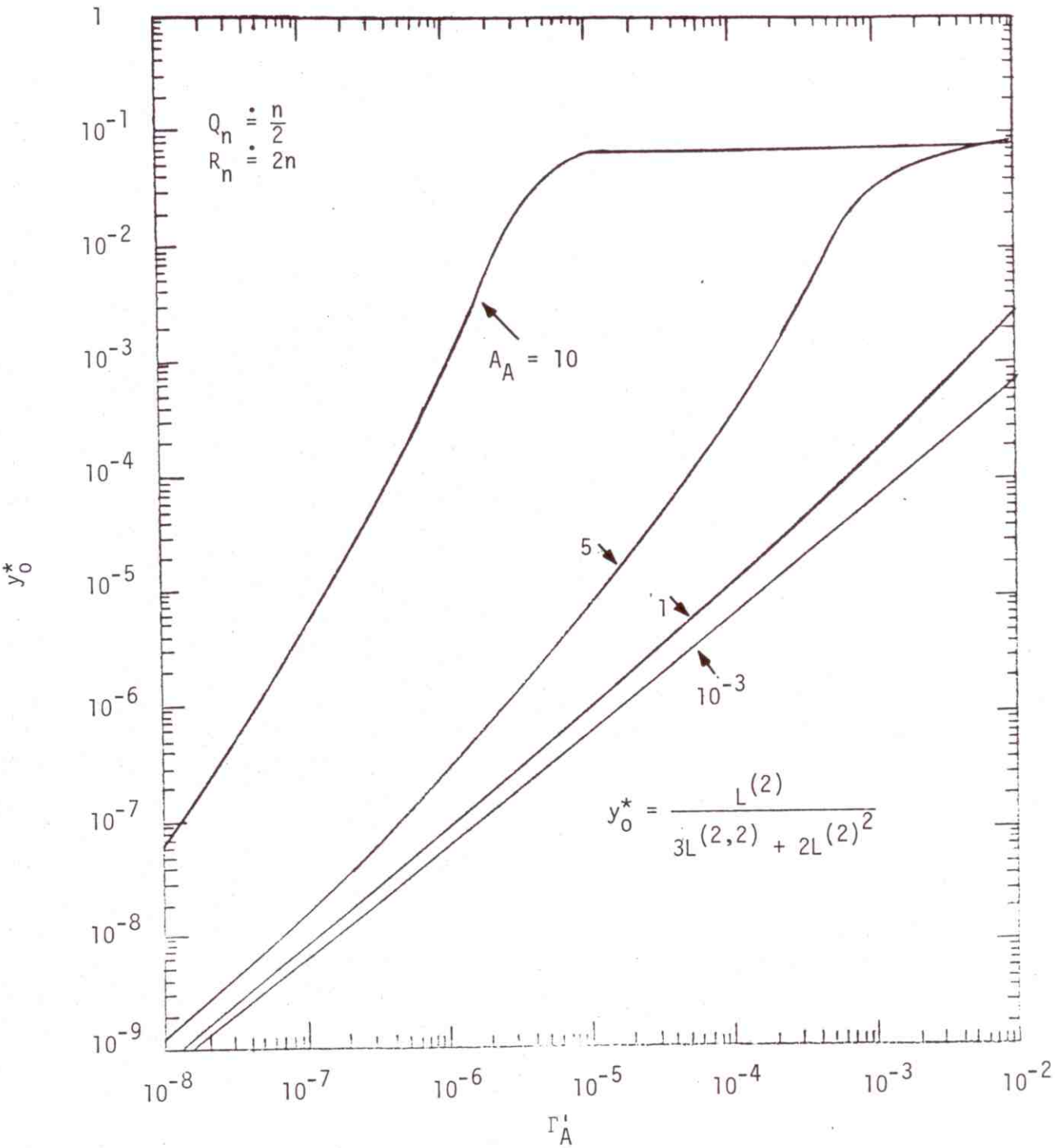

Figure 7.19. The bound, y_o^*, for incoherent detection of signals with fully coherent structure, in Class A EMI: ($Q_n \doteq n/2$, $R_n \doteq 2n$, $n \gg 1$, no, slow, or rapid fading); Eq. (7.24).

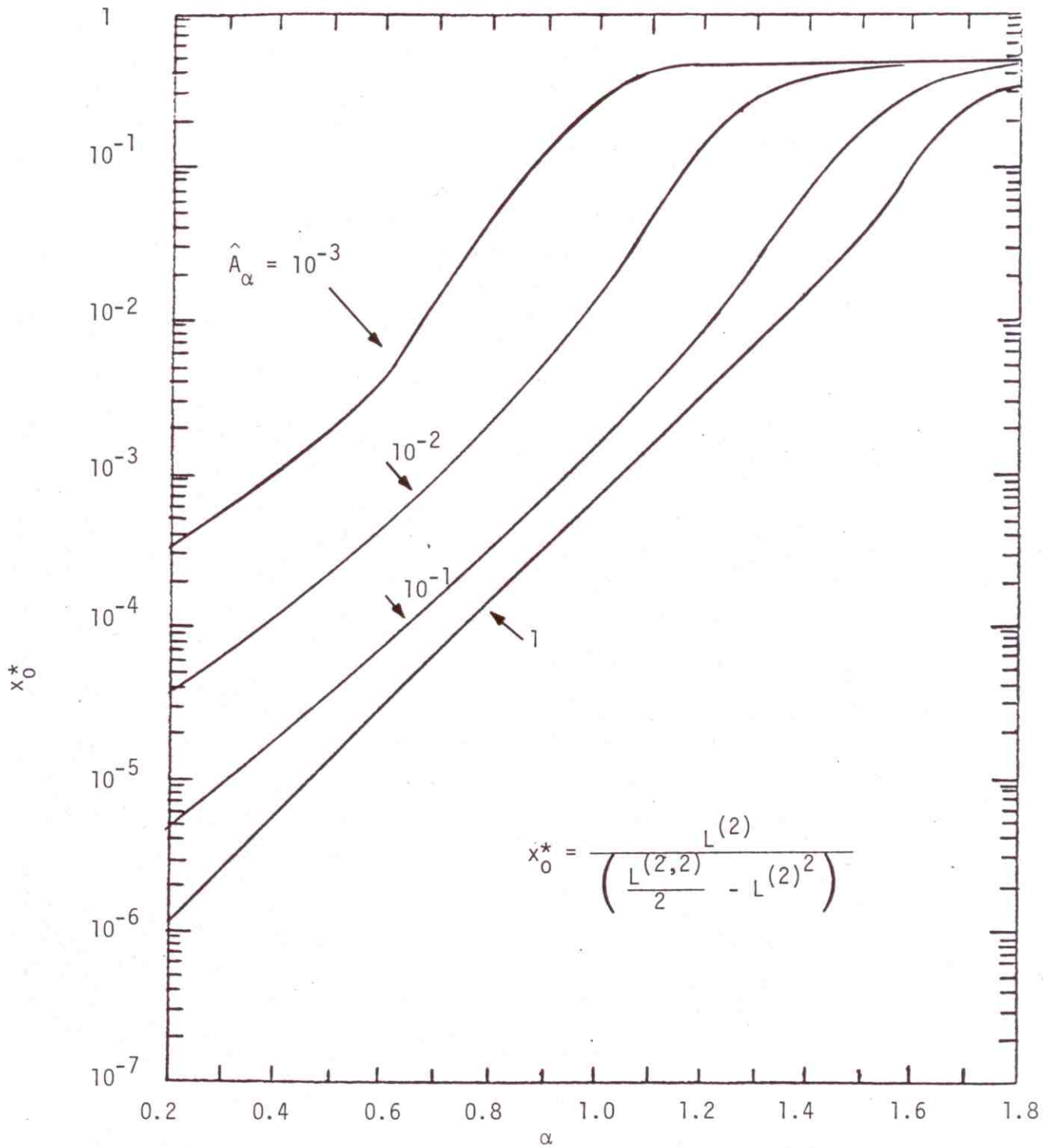

Figure 7.20. The bound, x_o^*, for coherent detection of (coherent) signals in Class B EMI, Eq. (7.23); (No or little fading: $\overline{a_o^2} \doteq \overline{a}_o^{\,2}$).

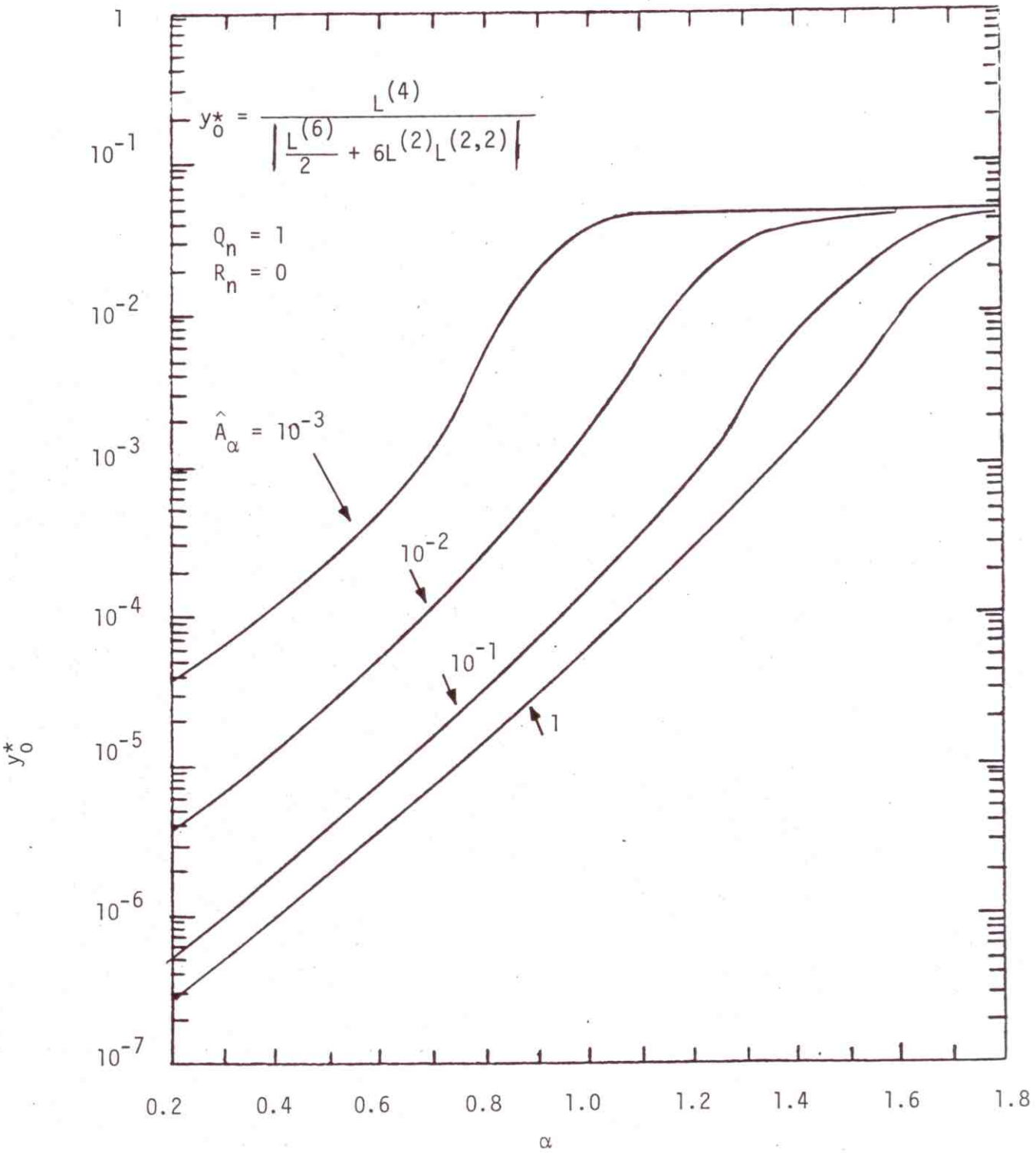

Figure 7.21. The bound, y_o^*, for incoherent detection of signals with fully incoherent structure in Class B EMI ($Q_n = 1$, $R_n = 0$), Eq. (7.24), arbitrary fading.

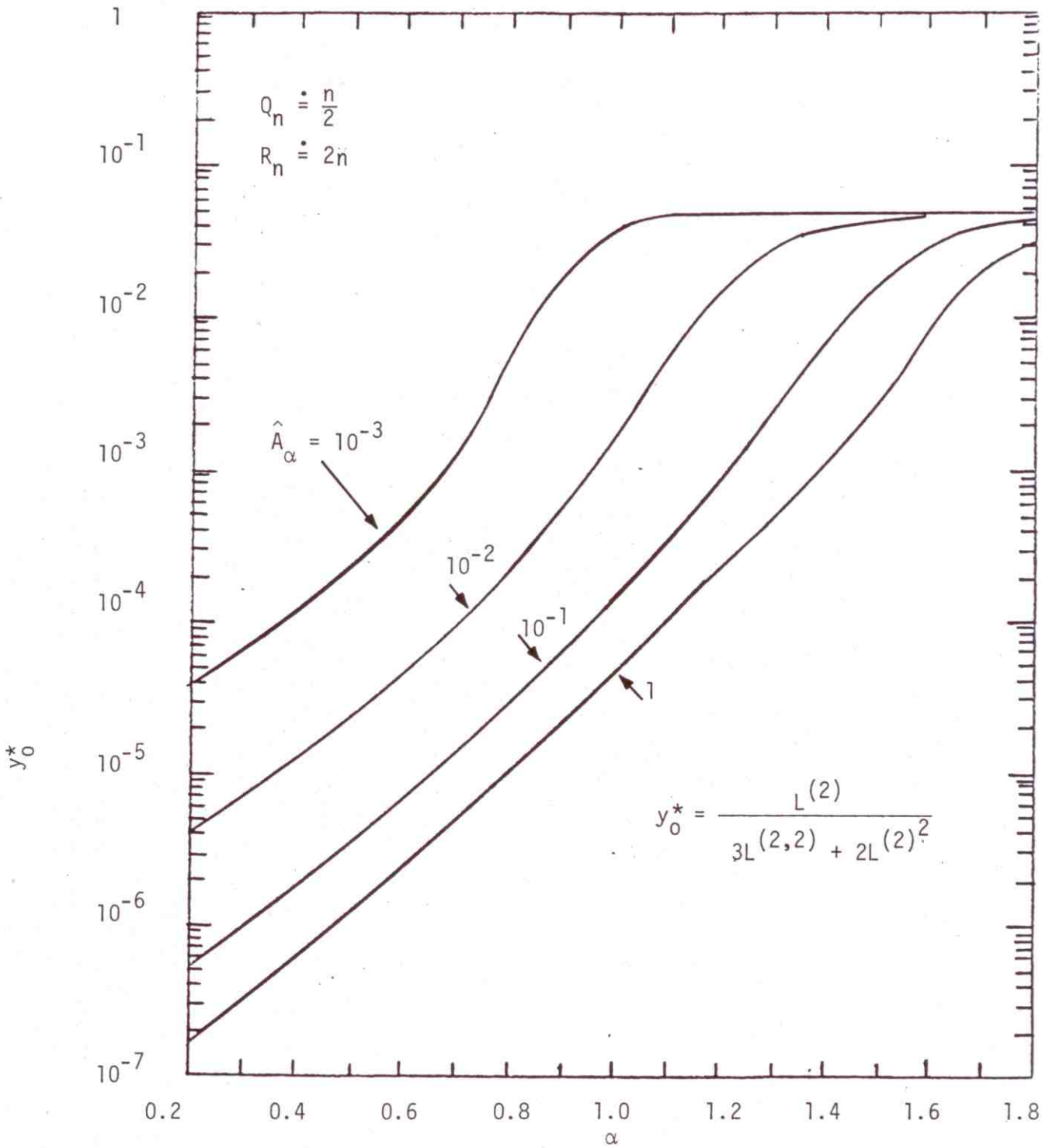

Figure 7.22. The bound, y_o^*, for incoherent detection of signals with fully coherent structure, in Class B EMI; ($Q_n \doteq n/2$, $R_n \doteq 2n$, $n \gg 1$, no, slow, or rapid fading) Eq. (7.24).

seek a combination of canonical performance results with specific elements whereby particular numerical values may be obtained, as in Section 7.5 following.

I. Canonical Suboptimum Performance Measures:

Analogous to (7.13) we can write directly from Eqs. (6.50), (6.51) in suboptimum threshold situations [cf. footnote p. 55].

$$P_D \cong \frac{p}{2}\{1+\Theta[\sqrt{\Phi_d^*}\, C^*_{N.P.} - \Theta^{-1}(1-2\alpha_F)]\} \ , \quad [\text{Eq. (6.50)}] \ , \tag{7.25}$$

and

$$P_e \cong \frac{1}{2}\{1-\Theta[\tfrac{1}{2}\sqrt{\Phi_d^*}\, C^*_{I.O.}]\} \ , \quad [\text{Eq. (6.51)}] \ , \tag{7.26}$$

respectively for correct signal detection, and error probability in the subsequent "communication" phase of detection decisions. Figures 7.23 and 7.24 give the canonical relations between P_D, P_e and the degradation factor, Φ_d^*, cf. Tables 6.1a,b, 6.2; (6.18), (6.38), (6.42a,b), etc. The relations (7.25), (7.26) are canonical equivalents of (7.13).

II. Various Degradation Factors, Φ_d^*:

In order to use (7.25), (7.26) in relation to specific signal, noise, and reception conditions we need the explicit forms of the degradation factor, Φ_d^*. These are readily summarized below, from Tables 6.1a,b, 6.2. We have

A. Simple Correlators: Φ_d^*, "on-off" signals:

(i). coherent reception:

$$\Phi_d^* = 1/L^{(2)} \ , \ [\text{Eq. (6.18)}]. \tag{7.27a}$$

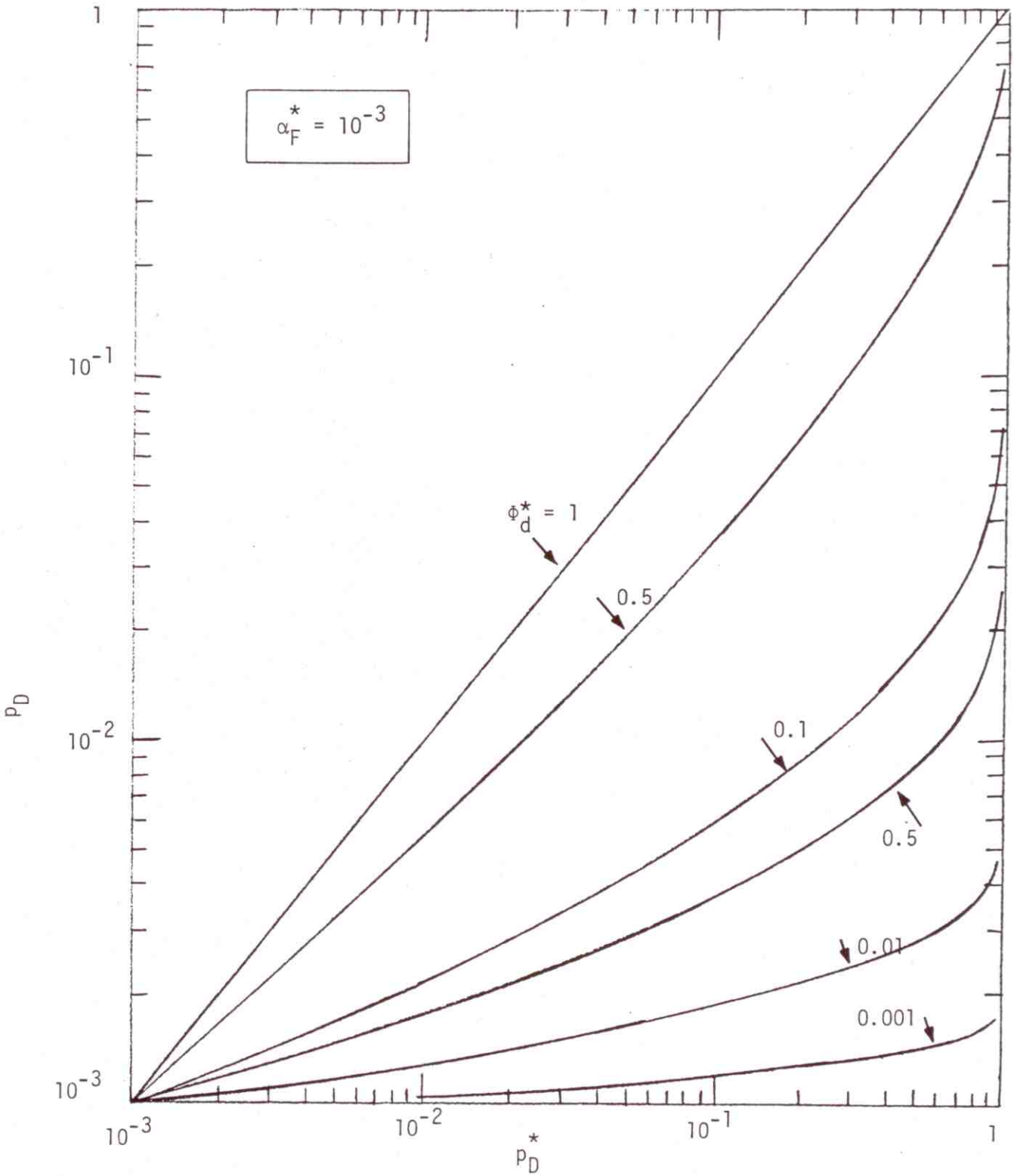

Figure 7.23a. Probability of detection versus optimum probability of detection for a false alarm probability of 10^{-3} and various degradation factors Φ_d^*, Equation (7.25).

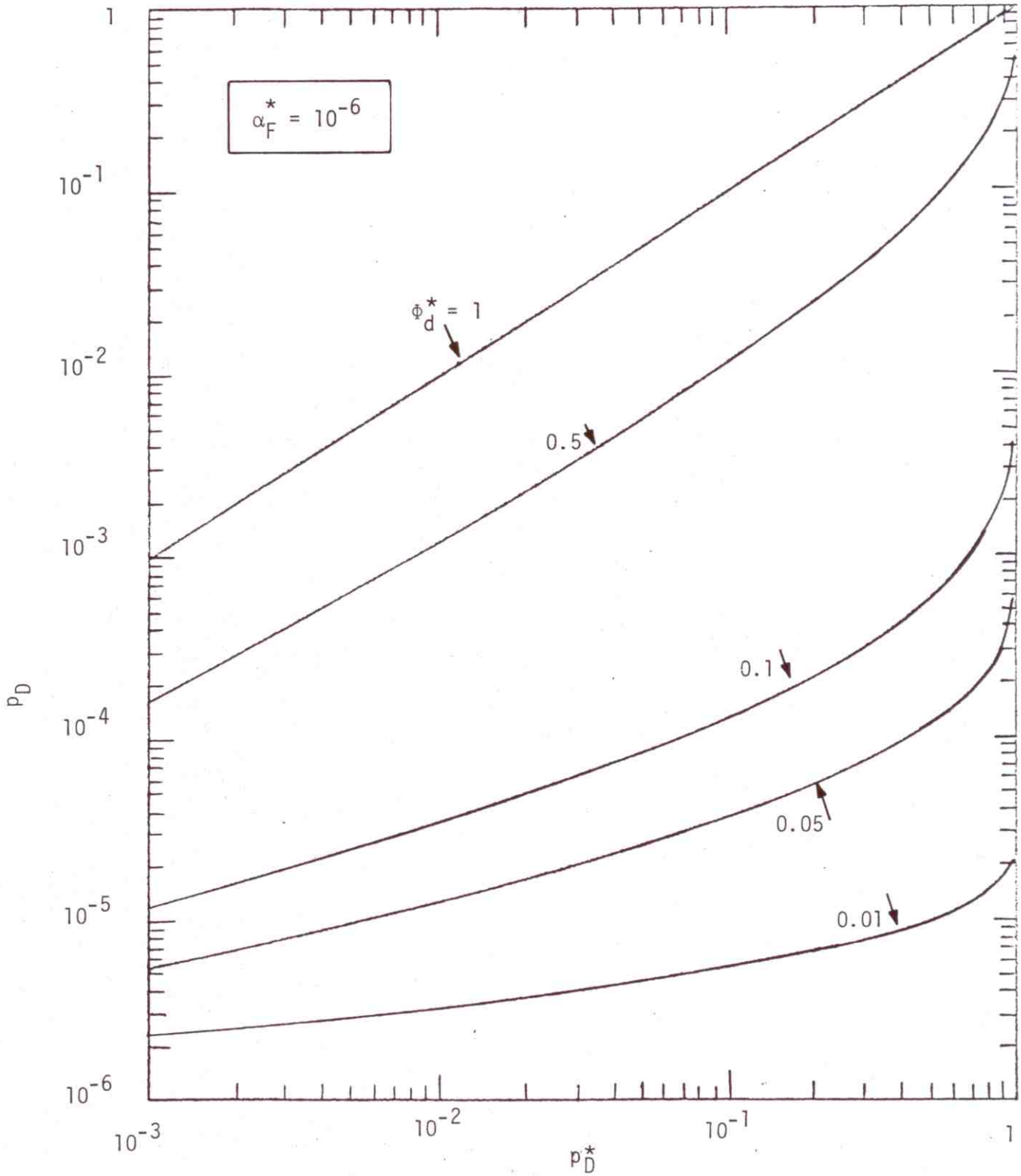

Figure 7.23b. Probability of detection versus optimum probability of detection for a false alarm probability of 10^{-6} and various degradation factors Φ_d^*, Equation (7.25).

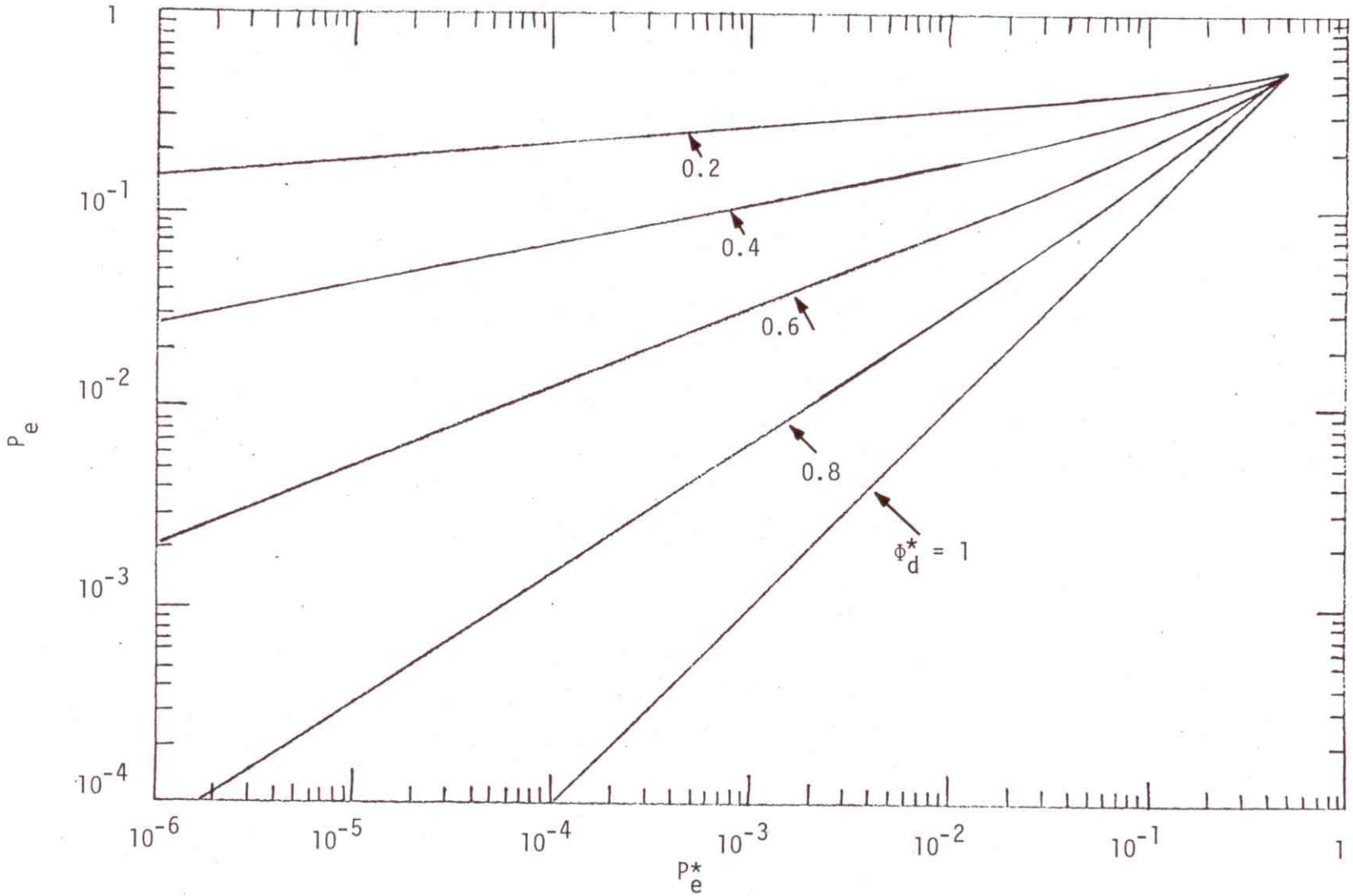

Figure 7.24. Probability of binary bit error versus optimum probability of error for various degradation factors Φ_d^*, Equation (7.26).

(ii). incoherent reception:

$$\begin{cases} \Phi_d^*\big|_{\text{incoh.struct.}} = 4/L^{(4)}(\overline{x^4}-1); \ [Q_n=1]; & (7.27b) \\ \Phi_d^*\big|_{\text{coh. struct.}} = 1/L^{(2)^2} \ ; \ [Q_n \simeq n/2 \gg 1, \text{ sinusoids}] \ . & (7.27c) \end{cases}$$

[For intermediate values of Q_n use Eq. (6.38).] For binary signals, we get

(iii). coherent reception

$$\Phi_d^{(21)^*} = 1/L^{(2)} \ , \text{ Eq. (6.21)] .} \qquad (7.28a)$$

(iv). incoherent reception

$$\begin{cases} \Phi_d^{(21)^*}\big|_{\text{incoh.struct.}} = 0, \text{ [Eq. (6.42b)]: (degenerate case: indistinguishable signals)} & (7.28b) \\ \Phi_d^{(21)^*}\big|_{\text{coh.struct.}} = 1/L^{(2)^2} \ , \ [Q_n^{(21)} \sim n; \text{ sinusoids.}] & (7.28c) \end{cases}$$

[Again, for intermediate values of $\hat{Q}_n^{(21)}$, $Q_n^{(21)}$, use (6.42a,b).]

B. Clipper-Correlators: Φ_d^*, "on-off" signals:

(i). coherent reception:

$$\Phi_d^* = \frac{4w_{1E}(0)^2}{L^{(2)}} \ ; \ [E = A,B \text{ here; Table 6.2}] \qquad (7.29a)$$

(ii). incoherent reception:

$$\begin{cases} \Phi_d^*\big|_{\text{incoh.struct.}} = [2w''_{1E}(0)]^2/L^{(4)}; \ [Q_n=1]; & (7.29b) \\ \Phi_d^*\big|_{\text{coh. struct}} = \left\{\dfrac{4w_{1E}(0)}{L^{(2)}}\right\}^2, \ [Q_n \approx n/2 >> 1, \text{ sinusoids}]. & (7.29c) \end{cases}$$

Again, for intermediate values of Q_n, see Table 6.2. Similarly, from Table 6.1d, 6.2 we get for binary signals

(iii). coherent reception:

$$\Phi_d^* = \left\{\frac{4w_{1E}(0)^2}{L^{(2)}}\right\}^2, \quad [E = A,B, \text{ here}], \text{ cf. (7.29a)} ; \qquad (7.30a)$$

(iv). incoherent reception:

$$\begin{cases} \Phi_d^*\big|_{\text{incoh.struct.}} = 0, \text{ cf. Sec. 2.4-4 [indistinguishable signals]} & (7.30b) \\ \Phi_d^*\big|_{\text{coh.struct.}} = \left[\dfrac{4w_{1E}(0)^2}{L^{(2)}}\right]^2, \ [Q_n^{(21)} \approx n >> 1, \text{ sinusoids}]. & (7.30c) \end{cases}$$

To implement the Φ_d^*'s numerically we need next $\overline{x^4}$, and $w_{1A}(0)$, $w_{1B}(0)$, and, similarly $w''_{1A}(0)$, $w''_{1B}(0)$. These are, for the 4th moment of Class A and B interference

$$\overline{x^4}\Big|_{A,B} = \frac{3}{8}\left\{\frac{\Omega_{4A,B}}{\Omega_{2A,B}^2(1+\Gamma'_{A,B})^2}\right\} + 2 \quad ; \quad \Omega_{4A,B} = \frac{A_{A,B}}{4}\left\langle \hat{B}^4_{oA,B}\right\rangle, \qquad (7.31)$$

where we may use the EMI scenario (3.6) to determine Ω_4, viz.

$$\Omega_{4A,B} = A_{A,B}\left\langle \frac{a^4 G_o^4}{4\lambda^{4\gamma}} \right\rangle = A_{A,B}\left\{ \frac{\overline{a^4}\langle G_o^4\rangle}{4} \left\langle \frac{1}{\lambda^{4\gamma}} \right\rangle \Big|_{A,B} \right\}. \tag{7.32}$$

From (3.11) we get directly

$$\left\langle \frac{1}{\lambda^{4\gamma}} \right\rangle \equiv C^{(4)}_{\mu,\gamma} = \left(\frac{2-\mu}{4\gamma+\mu-2}\right)\left(\frac{1-\alpha_o^{4\gamma+\mu-2}}{1-\alpha_o^{2-\mu}}\right) \alpha_o^{2-4\gamma-\mu} \lambda_1^{-4\gamma};\ \alpha_o \equiv \lambda_o/\lambda_1 \text{ [cf. Fig. (3.1)]} \tag{7.33}$$

for this general class of scenario. With the help of (3.10) we can then write

$$\overline{x^4}\Big|_{A,B} = \frac{3}{8}\left\{ \frac{A\,\frac{\overline{a^4}\langle G_o^4\rangle}{4} C^{(4)}_{\mu,\gamma}}{(A\,\frac{\overline{a^2}}{2}\langle G_o^2\rangle C^{(2)}_{\mu,\gamma} + \sigma_G^2)^2} + 2 \right\}_{A,B}. \tag{7.34}$$

[For example, with the scenario of Sec. 7 of Ref. [9], where $\underline{a}$ (or G_o) is rayleigh distributed, say $\underline{a}$ is, we have $\overline{a^4} = 2\overline{a^2}^2$, $\langle G_o^4\rangle = \langle G_o^2\rangle^2$, etc., with $\gamma = 2$, $\mu = 0$ and (7.34) reduces to

$$\overline{x^4}\Big|_{A,B} = \frac{3}{8}\left\{ \frac{2C^{(4)}_{\mu,\gamma}}{A\, C^{(2)2}_{\mu,\gamma}(1+\Gamma')^2} + 2 \right\}_{A,B} \doteq \frac{1}{4A\alpha_o^2}\Big|_{A,B} \quad (>>1);\ \alpha_o^2 << 1,\ \Gamma' << 1.] \tag{7.34a}$$

Similarly, we get from the noise pdf's (3.13), (3.14), (7.11):

$$\underline{\text{(Canonical):}}\quad w_{1A}(0)_{A+G} = e^{-A_A} \sum_{m=0}^{\infty} \frac{A_A^m (1+\Gamma'_A)^{1/2}}{m!\sqrt{2\pi}(m/A_A+\Gamma')^{1/2}},\ \text{cf. (3.13)} \tag{7.35a}$$

(quasi-canonical):

$$w_{1A}(0)_{A+G} = e^{-A_A \hat{g}_o} \sum_{m=0}^{\infty} \frac{(A_A \hat{g}_o)^m}{m!} \left\{ \frac{d}{\sqrt{4\pi\sigma_{om}^2}} + \hat{\Phi}(0)(0) \right\}, \text{ cf. (3.14),(3.14a).} \tag{7.35b}$$

For the Class B noise we have directly

$$w_1(0)_{B+G} \simeq \frac{1}{\pi\sqrt{\Omega_B}} \sum_{n=0}^{\infty} \frac{(-1)^n}{n!} \hat{A}_\alpha^n \, \Gamma\left(\frac{n\alpha+1}{2}\right) . \tag{7.36}$$

The second derivatives of the pdf's, w_1 above, are found similarly to be, for example,

(canonical):

$$w_1''(0)_{A+G} = -e^{-A_A} \sum_{m=0}^{\infty} \frac{A_A^m}{m! 2\hat{\sigma}_{mA}^2} \frac{1}{\sqrt{2\pi}\sqrt{2\hat{\sigma}_{mA}^2}} \tag{7.37}$$

$$w_1''(0)_{B+G} = -\frac{4}{\pi\Omega_B^{3/2}} \sum_{n=0}^{\infty} \frac{(-1)^n}{n!} \hat{A}_\alpha^n \, \Gamma\left(\frac{n\alpha+3}{2}\right) . \tag{7.38}$$

Figures 7.25, 7.26 show $w_1(0)_{A+G}$ (canon.), $w_1(0)_{B+G}$, Eqs. (7.35a), (7.36), for various ranges of parameters of these EMI models.

III. ARE's:

These are the Asymptotic Relative Efficiencies (ARE's) defined and derived in Sec. 6.3, IV above. We give here only the more important, limiting cases:

TABLE 7.1 ASYMPTOTIC RELATIVE EFFICIENCIES.

	ARE^2: coherent reception (Φ_d^*) ["on-off" + binary]	ARE^2: incoherent reception ["on-off"]
(1) simple correlator / optimum	$1/L^{(2)}$	$4/L^{(4)}(\overline{x^4}-1)$: incoh. sig. structures $1/L^{(2)2}$: coh.sig. struct. (n>>1)
(2) clipper correlator / optimum	$4w_{1E}(0)^2/L^{(2)}$	$2w''_{1E}(0)^2/L^{(4)}$: incoh. sig. struct. $\{4w_{1E}(0)^2/L^{(2)}\}^2$: coh. sig. struct. (n>>1)
(3) simple correlator / clipper correlator	$1/4w_{1E}(0)^2$	$2/w''_{1E}(0)^2(\overline{x^4}-1)$: incoh. sig. struct. $1/[4w_{1E}(0)^2]^2$: coh. sig. struct. (n>>1)

In the case of (symmetrical) binary reception (no or slow fading) in the incoherent detection mode, (1) and (2) above are zero, and (3) is 0/0 (indeterminate). For coherent signal structures, however, these ARE's are the same as for the "on-off" cases. We note, also, that here the $(ARE)_{inc} = (ARE)^2_{coh}$, and further, that in these limiting situations of large sample size (incoherent reception), the $(ARE)_{inc} = \Phi^*_{d,coh}$, $(n>>1)$, as well, cf. (7.27)-(7.30) above. (For intermediate cases where Q_n, $Q_n^{(21)}>1$ but are less than $(n/2, n)$ we must use the more complex formulae of Sec. 6.3, IV directly.)

Finally, Figures 7.27-7.30 show the (square of the) ARE's ($=\Phi^*_d$'s) here, for (1) and (2) of Table 7.1, for (canonical) Class A and Class B noise. The ARE ($=\sqrt{\Phi^*_d}$) for (3): [simple correlator/clipper correlator] may be obtained at once by subtracting, viz: $ARE_{(3)}(db) = [ARE_{(1)} - (ARE)_{(2)}]$ db. In general the clipper-correlators are much closer to optimum performance than are the simple correlators, when, as is the case here, the EMI is Class A or B noise. [But, regarding the use of ARE's as comparative performance measures, see the caveat at the end of Sec. 6.3.3, III.]